Optimization of secondary air operation parameters of waste incineration boiler based on response surface methodology

Applied Thermal Engineering 236 (2024) 121763

Contents lists available at ScienceDirect

Applied Thermal Engineering

journal homepage: www.elsevier.com/locate/apthermeng

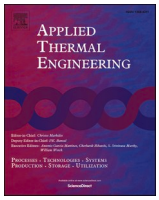

Research Paper

Optimization of secondary air operation parameters of waste incineration boiler based on response surface methodology

Minfeng Zheng [a,1], Jiakang Sun [b,1], Lingzhu Gong [a], Yaming Fan [a], Jiyuan Tu [c], Jingliang Dong [d,e,*]

[a] College of Eco-Environment and Urban Construction, Fujian University of Technology, Fuzhou 350118, China
[b] Fujian Snowman Co., Ltd, Fuzhou 350200, China
[c] School of Engineering, RMIT University, PO Box 71, Bundoora VIC 3083, Australia
[d] Institute for Sustainable Industries & Liveable Cities, Victoria University, P.O. Box 14428, Melbourne, VIC 3011, Australia
[e] First Year College, Victoria University, Footscray Park Campus, Footscray, VIC 3011, Australia

ARTICLE INFO

Keywords:
Numerical simulation
Secondary air
NO_x concentration
Thermal efficiency
Response surface design

ABSTRACT

To reduce the NO_x emission concentration of waste incineration boilers and improve the thermal efficiency of incinerators, the combustion process of a 600 t/d incineration boiler was numerically investigated. First, the influences of the secondary air injection angle, velocity and temperature on the NO_x concentration at the waste incineration boiler outlet and the thermal efficiency of the incinerator were analyzed through a single factor simulation test. Then, coupling optimization of key operating parameters, including the secondary air injection angle, velocity and temperature, was conducted via the response surface design method to obtain the specific functional relationships between outlet NO_x concentration, incinerator thermal efficiency, front wall secondary air injection angle, rear wall secondary air velocity and secondary air temperature, as well as the optimal operating parameters for the boiler. The results showed that when the secondary air injection angle of the front wall ranges from 68°~80° and the secondary air injection angle of the back wall is 67°, the minimum NO_x concentration is 142.23 mg/m^3, and the maximum thermal efficiency of the incinerator reaches 85.51 %. When the secondary air velocity at the front wall is 42 m/s and the secondary air velocity at the back wall ranges from 42 ~ 66 m/s, the NO_x concentration at the outlet is the lowest at 140.05 mg/m^3, and the thermal efficiency of the incinerator is the highest at 85.63 %. When the secondary air temperature ranges from 297.16 ~ 309.16 K, the NO_x concentration at the outlet is the lowest at 155.45 mg/m^3, and the thermal efficiency of the incinerator is the highest at 84.64 %. The secondary air injection angle, velocity and temperature impose significant effects on the NO_x concentration at the outlet and thermal efficiency of the incinerator. The optimal parameters, as determined in the multifactor simulation test, include a 77° secondary air injection angle of the front wall, 69 m/s secondary air velocity at the back wall, and 297.15 K secondary air temperature. Under these conditions, the NO_x concentration at the outlet is 134.98 mg/m^3, and the thermal efficiency of the incinerator reaches 86.11 %. This study has important guiding significance for reducing pollution and improving the efficiency of waste incineration boilers.

1. Introduction

Rapid urbanization and economic growth have posed notable environmental hazards due to the very large amount of municipal solid waste generation [1,2]. According to a statical report, the annual domestic waste amount in China exceeded 2 billion tons in 2021 [3]. How to properly manage this domestic waste remains a challenge. At present, the primary ways to manage domestic waste in cities include landfilling, incineration and composting [4]. The conventional landfilling method may pose long term threats to groundwater and surface water bodies that are hydrologically connected. Another method of treating municipal solid waste is composting, a biological process in which the organic portion of waste is allowed to decompose under carefully controlled conditions. However, the low processing speed cannot meet the current market demand. Finally, incineration is a mainstream method for the

* Corresponding author at: Institute for Sustainable Industries & Liveable Cities, Victoria University, P.O. Box 14428, Melbourne, VIC 3011, Australia.
E-mail address: jingliang.dong@vu.edu.au (J. Dong).
[1] The authors contributed equally to this work.

https://doi.org/10.1016/j.applthermaleng.2023.121763
Received 19 May 2023; Received in revised form 20 September 2023; Accepted 7 October 2023
Available online 9 October 2023

Nomenclature

a	Base ash content percentage
b	Combustible content of fly ash, %
c	Base low calorific value, kJ·kg^{-1}
D_g	Diffusion coefficient
D_{ed}	The rated power
D_{sc}	The actual power
$F(U_g)$	The resistance of the gas in the × direction, N
$F(V_g)$	The resistance of the gas in the y direction, N
$F(W_g)$	The resistance of the gas in the z direction, N
g	Gas
H_g	Enthalpy value, J/kg
j	Type of gas
m	Calculation coefficient, 0.44
n	Calculation coefficient, 3.55
P_g	Static pressure, Pa
Q_h	Heat source, W/m3
$S_{g,j}$	Mass source term, kg/m^3·s
T_g	Temperature, K
T_{out}	exhaust gas temperature, K
T_{in}	fiducial temperature, K
U_g	Velocity in the x-axis, m/s
V_g	Velocity in the y-axis, m/s
W_g	Velocity in the z-axis, m/s
x	Along the grate, m
$Y_{g,j}$	The mass fraction of the component
y	Along the height of the incinerator, m
z	Along the depth of the incinerator, m
φ	Bed garbage voidage
ρ_g	Mass density of flue gas, kg/m^3
α	Excess air number
λ	Thermal conductivity, W/m·K
η	Thermal efficiency of incinerator, %
Δq_2	Exhaust heat loss rate, %
Δq_3	Heat loss rate of incomplete combustion of gas, %
Δq_4	Heat loss rate of incomplete combustion of solids, %
Δq_5	Heat dissipation loss rate, %
Δq_{5ed}	Heat dissipation loss rate when the rated power is not less than 75 %, %
Δq_6	Physical heat loss rate of ash, %

comprehensive treatment of urban combustible solid waste, which not only efficiently disposes of waste but also utilizes waste [5,6]. However, with the continuous expansion of the waste incineration treatment scale, the output of nitrogen oxides and other pollutants is higher than before, and it is difficult to improve the thermal efficiency of boilers, so more efficient waste incineration technology is needed [7]. At present, efficient waste incineration can be realized by optimizing the operational parameters of incineration boilers, and optimization of the air distribution parameters of the incinerator is the main method to enhance the operation parameters of the boiler [8,9]. The air distribution parameters of the incinerator refer to the air supply, suction (ventilation), primary air and secondary air.

Regarding the status of research on the air distribution in incineration boilers, current air distribution-related studies mainly focus on the ratio of primary air, secondary air and exhaust air [10] the influence of the secondary air injection position on the combustion status of combustible components in the furnace [11] and consider the optimization of the structure and parameters by analyzing flow field changes [12,13]. Many relevant research results have been obtained [14]. By studying the air volume ratio of secondary air and exhaust air, the optimal air volume ratio can be determined. Under the condition of the optimal ratio, the NO_x concentration can be reduced by 3.3 % relative to the original condition [15]. By studying the influence of the ratio of primary and secondary air on the combustion process, it has been found that when the secondary air volume of the front arch is increased, the turbulence intensity in the furnace increases, which is conducive to extending the residence time of flue gas in the incinerator and the mixing of combustible components and oxygen to achieve full combustion [16]. By studying the velocity of secondary air, it has been shown that the optimized incinerator achieves favorable combustion conditions and low pollutant emission concentrations. The NO_x emissions of domestic waste incinerators have been numerically simulated, and NO_x emissions have been optimized by analyzing flow field changes [17]. By analyzing and evaluating the NO_x emission characteristics of lignite in a single-angle furnace with graded combustion, it has been experimentally shown that graded air combustion can significantly reduce NO_x emissions [18].

Above studies suggest that the current research methods for boiler operation parameters are too simplistic, relying heavily on the single factor control variable method to study relevant factors, leading to limited applicability. Few researchers have studied the secondary air operation parameters concerning the influence of its injection angle, wind speed and temperature on outlet NO_x concentration and incinerator thermal efficiency. Seeking the specific functional relationship between these factors remains underexplored. Therefore, in this paper, UDF was used to load the actual velocity, temperature and components of flue gas above the bed into FLUENT as boundary conditions for coupling calculation. First, the optimal operating conditions of the secondary air injection angle, wind speed and temperature were determined via a single factor test. Then, the NO_x concentration at the outlet and the thermal efficiency of the incinerator were analyzed via the response surface method, and the influence of the interaction between each factor on the NO_x concentration at the outlet and the thermal efficiency of the incinerator was studied. A specific functional relationship between the NO_x concentration at the outlet and the thermal efficiency of the incinerator as well as various factors was established. The response surface model was used to predict each factor, and a simulation test was performed according to the predicted values to select the optimal secondary air operation conditions, which could provide a reference for the efficient operation of municipal solid waste (MSW) incineration power generation boilers.

2. Materials and methods

2.1. Object of study

A 600 t/d waste incinerator in Fuzhou was adopted as the research object, and because the structure of the waste incinerator is highly complex, to make the simulation process more convenient, the installation position of the incinerator burner, feed port, SNCR nozzle and drum and other structures were simplified to facilitate the numerical simulations. The structural diagram of the municipal solid waste incineration boiler is shown in Fig. 1. The total length of the grate is 9.5 m, and the inclination angle of the grate is 24°. Under the grate is a primary air supply ash hopper. The speed and temperature of primary air are controlled by the pressure machine and steam air preheater, respectively, and secondary air is directly discharged into the furnace through the secondary air nozzle. There are 21 secondary air intakes on the front wall, and the spacing between the air intakes is 0.57 m. The rear wall contains 16 secondary air intakes, and the spacing between the air intakes is 0.74 m.

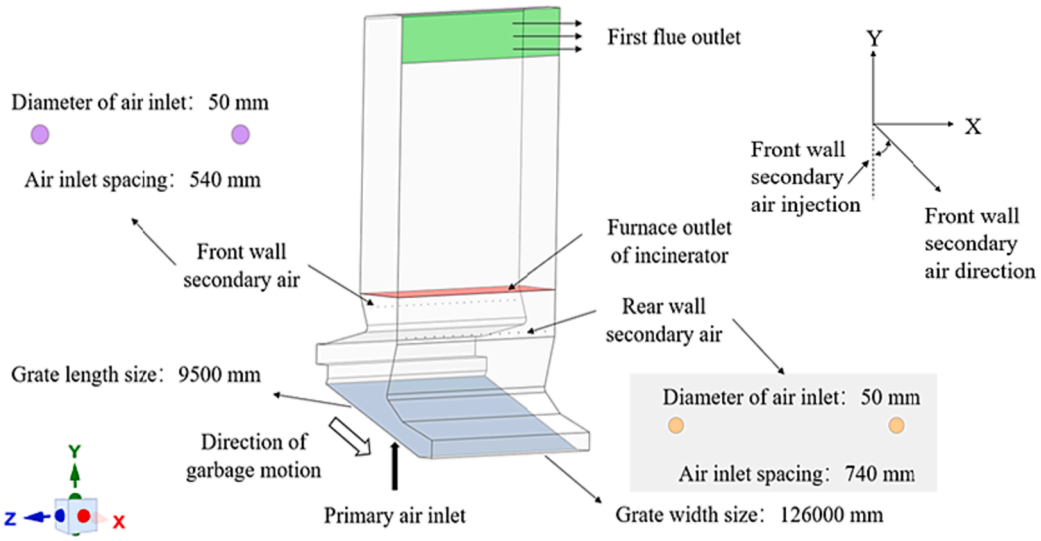

Fig. 1. Drawing of the structure of an incineration boiler for municipal solid waste.

2.2. Mathematic model

In FLUENT software, the following equations are combined to obtain gas phase combustion, heat transfer and mass transfer:

Equation of continuity:

$$\frac{\partial(\varphi\rho_g U_g)}{\partial x}+\frac{\partial(\varphi\rho_g V_g)}{\partial y}+\frac{\partial(\varphi\rho_g W_g)}{\partial z}=S_{g,j} \tag{1}$$

X direction momentum equation:

$$\frac{\partial(\varphi\rho_g U_g U_g)}{\partial x}+\frac{\partial(\varphi\rho_g V_g U_g)}{\partial y}+\frac{\partial(\varphi\rho_g W_g U_g)}{\partial z}=-\frac{\partial P_g}{\partial x}+F(U_g) \tag{2}$$

Y direction momentum equation:

$$\frac{\partial(\varphi\rho_g U_g V_g)}{\partial x}+\frac{\partial(\varphi\rho_g V_g V_g)}{\partial y}+\frac{\partial(\varphi\rho_g W_g V_g)}{\partial z}=-\frac{\partial P_g}{\partial y}+F(V_g) \tag{3}$$

Z direction momentum equation:

$$\frac{\partial(\varphi\rho_g U_g W_g)}{\partial x}+\frac{\partial(\varphi\rho_g V_g W_g)}{\partial y}+\frac{\partial(\varphi\rho_g W_g W_g)}{\partial z}=-\frac{\partial P_g}{\partial z}+F(W_g) \tag{4}$$

Energy equation:

$$\frac{\partial(\varphi\rho_g U_g H_g)}{\partial x}+\frac{\partial(\varphi\rho_g V_g H_g)}{\partial y}+\frac{\partial(\varphi\rho_g W_g H_g)}{\partial z}=\frac{\partial}{\partial x}\left(\lambda_g\frac{\partial T_g}{\partial x}\right)+\frac{\partial}{\partial y}\left(\lambda_g\frac{\partial T_g}{\partial y}\right)+\frac{\partial}{\partial z}\left(\lambda_g\frac{\partial T_g}{\partial z}\right)+Q_h \tag{5}$$

Component transport equation:

$$\frac{\partial(\varphi\rho_g U_g Y_{g,j})}{\partial x}+\frac{\partial(\varphi\rho_g V_g Y_{g,j})}{\partial y}+\frac{\partial(\varphi\rho_g W_g Y_{g,j})}{\partial z}=\frac{\partial}{\partial x}\left(D_g\frac{\partial(\varphi\rho_g Y_{g,j})}{\partial x}\right)+\frac{\partial}{\partial y}\left(D_g\frac{\partial(\varphi\rho_g Y_{g,j})}{\partial x}\right)+\frac{\partial}{\partial z}\left(D_g\frac{\partial(\varphi\rho_g Y_{g,j})}{\partial z}\right)+S_{g,j} \tag{6}$$

Regarding the simulated area in this paper, gas phase combustion above the bed was simulated in FLUENT software. In the simulation process, flue gas transport in the furnace adopts the component transport model [19,20], combustion adopts the finite-rate/eddy dissipation model [21], gas-phase turbulence adopts the RNG k-ε turbulence model [22,23], radiation heat transfer adopts the P1 model [24], and the governing equation adopts the SIMPLE algorithm for solution purposes.

Three commonly used turbulence models, namely RNG k-ε, Realizable k-ε, and SST k-ω, were considered for this study. The RNG model demonstrates superior accuracy in calculating flow fields with substantial gradients and incorporates an analytical formula for determining the turbulence Prandtl number, making it well suited to our specific conditions. All three turbulence models were configured, with other settings unchanged.

Simulation tests were conducted using Fluent software, and the simulation results were compared with actual values for temperature at the exit of the first flue, temperature in the middle of the first flue, and temperature at the exit of the furnace. The operating conditions are as follows: the average inlet flue gas temperature is 1000.48 K, the average inlet flue gas velocity is 0.73 m/s, the front wall secondary air injection Angle is 74°, the rear wall secondary air injection Angle is 67°, the front wall secondary air velocity is 42 m/s, the rear wall secondary air velocity is 42 m/s, and the secondary air temperature is 301.15 K. The results, as presented in Table 1, indicate that the RNG k-ε model exhibits closer agreement with the actual values and offers higher reliability than the other two models. Consequently, this paper employs the RNG k-ε turbulence model for a comprehensive analysis of turbulent gas flow in the incinerator [25].

The waste used in this research is domestic waste in Fuzhou. At the initial stage, multiple groups of investigation and analysis were conducted to achieve proximate and ultimate analysis of the waste treated at the waste incineration power plant. The analysis results are listed in

Table 1
Numerical predictions yielded by different turbulence models.

Turbulence model	Parameter	Value of simulation	True value	Error /%
RNG k-ε model	First flue outlet temperature /K	1218.28	1166.15	4.47
	Middle temperature of first flue /K	1241.44	1290.75	3.82
	Furnace outlet temperature /K	1282.56	1315.15	2.47
Realizable k-ε model	First flue outlet temperature /K	1232.76	1166.15	5.71
	Middle temperature of first flue /K	1253.95	1290.75	2.85
	Furnace outlet temperature /K	1276.31	1315.15	2.95
SST k-ω model	First flue outlet temperature /K	1216.43	1166.15	4.31
	Middle temperature of first flue /K	1232.62	1290.75	4.50
	Furnace outlet temperature /K	1268.87	1315.15	3.55

Table 2
Proximate analysis and Ultimate analysis of MSW.

Proximate analysis	Wt (%)	Margin of error (%)	Ultimate analysis	Wt (%)	Margin of error (%)
			C	56.62	3
Moisture	49.22	3	H	9.43	2
Volatiles	28.18	4	O	30.85	3
Fixed carbon	5.96	2	N	0.32	0.2
Ash content	16.64	2	S	0.61	0.2
			Cl	2.17	0.4

Table 2. The error limits of proximate and ultimate analysis slightly influence the components of flue gas. However, the waste treated at the waste incineration power plant originates from several areas in Fuzhou city, and after fermentation and crushing, the ultimate analysis results remain relatively stable, so the error limits impose little influence on the components of flue gas. Therefore, proximate analysis and ultimate analysis of the waste used in this paper provide reliability and practical significance.

CH_4, CO and H_2 are the main combustible gases produced during waste drying and pyrolysis, while the main components of flue gas also contain N_2, CO_2, H_2O and O_2. As the content of H_2 produced in the process of waste drying and pyrolysis is very small, and the H_2 combustion reaction is very complex, the simplified chemical reaction process is adopted in the combustion simulation, and the H_2 chemical reaction is not considered. The gas phase combustion reaction equation and kinetic rate involved in this paper are shown in Table 3.

In this paper, Fluent standard model was used to represent the chemistry of NO_x. In more detail, the component transport equation was used to describe the chemical dynamics. The turbulent-chemical interaction was modelled using the "finite rate/eddy dissipation" model. The eddy dissipation model assumes that the reaction rate is influenced by turbulent mixing, which requires less computational resources. Chemical kinetics primarily determine the chemical reaction of NO_x in this simulation, while turbulence mainly increases airflow turbulency, extends the residence time of flue gas in the furnace, and ensures complete combustion of the combustible components. As such, turbulence has an auxiliary effect on chemical dynamics in this process.

In the process of waste incineration, the main form of NO_x is NO, accounting for about 90 %. Because the generation of prompt NO_x requires oxygen-rich conditions, combined with the combustion condition of waste incinerator, it can be seen that the generation of prompt NO_x is very small, so thermal NO_x and fuel NO_x are mainly considered in the simulation. The formation of thermal NO_x is primarily influenced by temperature, with a significant increase in NO_x production occurring when combustion temperatures exceed 1800 K. However, since waste incineration typically occurs at temperatures below this threshold, thermal NO_x is not a major contributor to the overall nitrogen oxide emissions from waste incineration facilities. In fact, thermal NO_x only accounts for approximately 10 % of total NO_x emissions. During the waste incineration process, the nitrogen in the fuel undergoes pyrolysis at low temperatures, which produces intermediate product groups such as N, CN, and HCN. These intermediates then oxidize into NO_x at temperatures ranging from 600 ~ 800℃, resulting in a significant amount of fuel NO_x emissions. At higher temperatures, the rate of NO generation slows down, making fuel NO_x the main form of NO_x emissions during waste incineration, accounting for approximately 90 % of total nitrogen oxide emissions.

Table 3
The reaction of gas phase combustion and its corresponding kinetic rate.

NO.	Reactions	Kinetic rates
R1	$CH_4 + 0.5O_2 \rightarrow CO + 2H_2$	$R_{CH_4} = 5.012 \times 10^{11} exp\left(\frac{-2 \times 10^8}{RT}\right) C_{CH_4}^{0.7} C_{O_2}^{0.8}$
R2	$CH_4 + 1.5O_2 \rightarrow CO + 2H_2O$	$R_{CH_4} = 5.012 \times 10^{11} exp\left(\frac{-2 \times 10^8}{RT}\right) C_{CH_4}^{0.7} C_{O_2}^{0.8}$
R3	$CO + 0.5O_2 \rightarrow CO_2$	$R_{CO} = 2.239 \times 10^{12} exp\left(\frac{-1.702 \times 10^8}{RT}\right) C_{CO} C_{O_2}^{0.25} C_{H2O}^{0.5}$

The formation mechanism of thermal NO_x is as follows:

$$N_2 + O \rightarrow NO + N \quad (7)$$

$$N + O_2 \rightarrow NO + O \quad (8)$$

The chain reaction of NO and NO_2 at high temperature is as follows:

$$N_2 + O_2 \rightarrow 2NO \quad (9)$$

$$NO + 0.5O_2 \rightarrow NO_2 \quad (10)$$

The generation rate of NO in thermal NO_x is calculated by Zeldovich mechanism model, and the generation rate is as follows:

$$R_{NO} = 3.0 \times 10^{14} exp\left(\frac{-5.42 \times 10^5}{RT}\right) C_{N_2} C_{O_2}^{0.5} \quad (11)$$

The generation mechanism of fuel NO_x is more complex than that of thermal NO_x, and the process can be simplified as a competition process for intermediate products. The intermediate products are generated by the pyrolysis of garbage and nitrogen-containing compounds. If the intermediate products are oxidized by oxygen, NO will be produced; if they are returned by NO, nitrogen will be produced.

Assuming that the intermediates are only HCN and NH_3, the generation rates of NO and N_2 in fuel NO_x are calculated using the DeSoete mechanism model, and the generation rates of NO and N_2 are as follows:

$$R_{NO} = 4.0 \times 10^6 exp\left(\frac{-1.344 \times 10^5}{RT}\right) C_{HCN} C_{NH_3} C_{O_2}^{0.5} \quad (12)$$

$$R_{N_2} = 1.8 \times 10^6 exp\left(\frac{-1.344 \times 10^5}{RT}\right) C_{HCN} C_{NH_3} C_{NO}^{0.5} \quad (13)$$

2.3. Mesh generation

In this paper, the height of the waste incineration boiler body is 27.6 m, the depth is 12.6 m, the width is 7.6 m, and the width of the first flue is 3.55 m. The grate has 4 rows and 19 columns along the direction of garbage movement, with an effective size of 9.162 m × 12.6 m. The grid division of the waste incineration boiler is shown in Fig. 2(a). The grid adopts an unstructured tetrahedral grid with a cell size of 0.15 m. As the secondary air tuyere is small, the grid is encrypted at the position of the tuyere. The grid independence study in Fig. 2(b) was conducted under the following operating conditions: an average inlet flue gas temperature of 1000.48 K, an average inlet flue gas velocity of 0.73 m/s, a front wall secondary air injection angle of 74°, a rear wall secondary air injection angle of 67°, front wall secondary air velocity at 42 m/s, rear wall secondary air velocity at 42 m/s, and a secondary air temperature of 301.15 K. As can be seen from Fig. 2b, when the total number of cells falls within the range of 3.1 to 3.8 million, the simulation results remain stable. All unstructured mesh elements have a maximum skewness below 0.8, a Jacoby ratio close to 1, and an average orthogonal quality of 0.86, indicating that the computational mesh is of high quality. Therefore, a total of approximately 3.4 million grids were utilized in the present study to ensure both the accuracy of the simulation and computational efficiency.

2.4. Boundary conditions

In this paper, the boundary conditions at the entrance are obtained from field tests, and the field test results are shown in Fig. 3-6 below. The distribution of measured flue gas composition mass fraction along the length of the grate is shown in Fig. 3 (data are collected from the primary

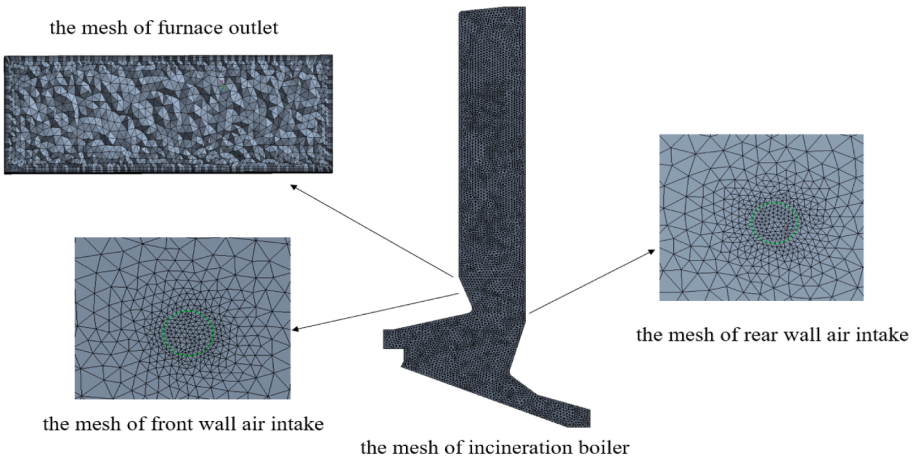

(a)

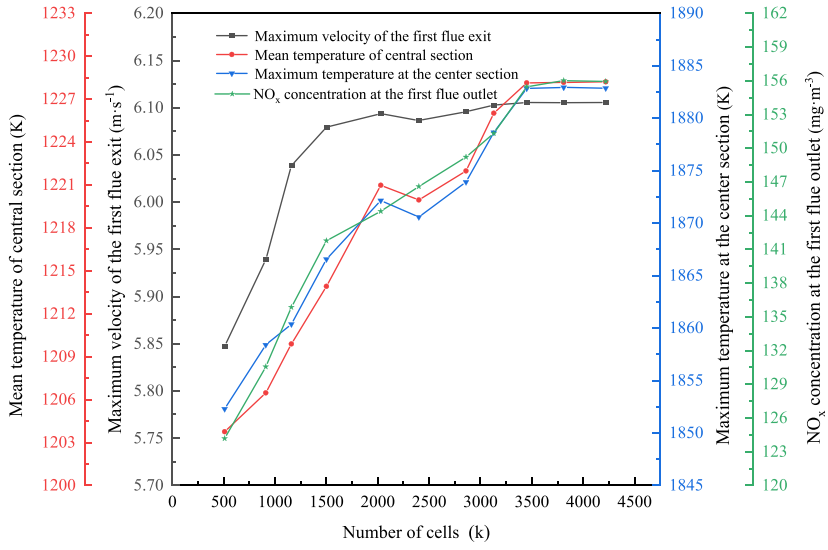

(b)

Fig. 2. (a) Computational grid and (b) mesh independence verification of the incineration boiler.

inlet surface, as shown in Fig. 1), and the average mass fractions of CH_4, CO, O_2, CO_2 and H_2O at the inlet boundary are 0.37 %, 1.43 %, 11.98 %, 14.48 % and 14.18 %, respectively. Since waste combustion entails the four stages of drying, pyrolysis, combustion and burnout, the water content in waste gradually decreases in the drying process. CH_4 is produced during waste pyrolysis and then burned, so the CH_4 content first increases and then decreases. At the combustion stage, local hypoxia leads to the production of CO. Then, with increasing oxygen content, CO is burned, so the CO content first increases and then decreases, while the CO_2 content first increases and then decreases with the combustion of CO and CH_4. Waste incineration consumes a large amount of oxygen at the pyrolysis and combustion stages, after which the waste enters the burnout stage, so the O_2 content first decreases and then increases. The flue gas velocity profile along the grate length is shown in Fig. 4 (the primary inlet is shown in Fig. 1), with an average velocity of 0.73 m/s. Waste must first be dried and pyrolyzed, which requires a large amount of heat. The velocity of flue gas first gradually increases, and the waste is then burned, which results in a decrease in heat. Therefore, the flue gas velocity starts to decrease, after which it increases, and the burnout stage is entered, where the required amount of oxygen decreases and the flue gas velocity gradually decreases. The flue gas temperature profile along the grate length is shown in Fig. 5 (the primary inlet is shown in Fig. 1), with an average temperature of 1000.48 K. Waste is dried, pyrolyzed and then burned, and the burnout stage commences, so the temperature rises first and then decreases along the grate. The concentration distribution of NO and HCN along the bed length is shown in Fig. 6 (the primary inlet is shown in Fig. 1). HCN is produced mainly at the grate from 2 ~ 5 m, i.e., the volatilization analysis stage. NO is produced largely at the grate from 3.5 ~ 8 m, i.e., the fixed carbon combustion stage, if all input HCN and NO form NO_x, the estimated boiler NO_x emission would be 176.53 mg/m^3. Secondary air is air with a normal temperature, and the speed inlet is adopted. The speed is 42 m/s, and the temperature is 301.15 K. The first flue outlet adopts a pressure outlet, the furnace is surrounded by adiabatic boundary conditions, the first flue is surrounded by constant-temperature boundary conditions, and the temperature is 740 K. The waste used in this study has an average low calorific value of 7574 kJ/kg, which results in a calculated boiler heat load of 48.92 MW. The model grate gas has a heat value of 6588.73 kJ/kg, and all the combustible components in the flue gas above the grate are fully burned and release 3108.52 kJ/kg.

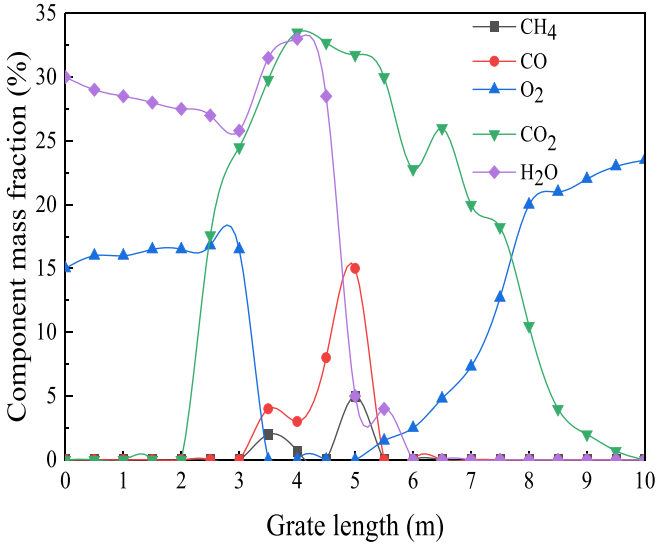

Fig. 3. Measured composition mass fraction profiles of flue gas along the grate length (data are collected from the primary inlet surface shown in Fig. 1).

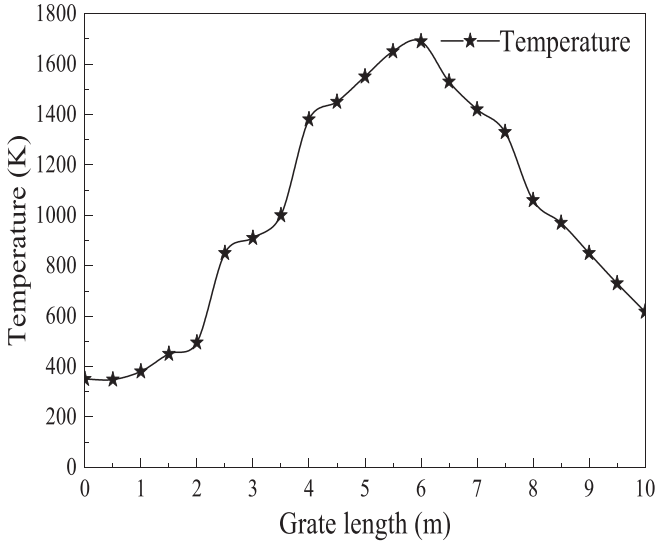

Fig. 5. Flue gas temperature profile along the grate length (the primary inlet is shown in Fig. 1).

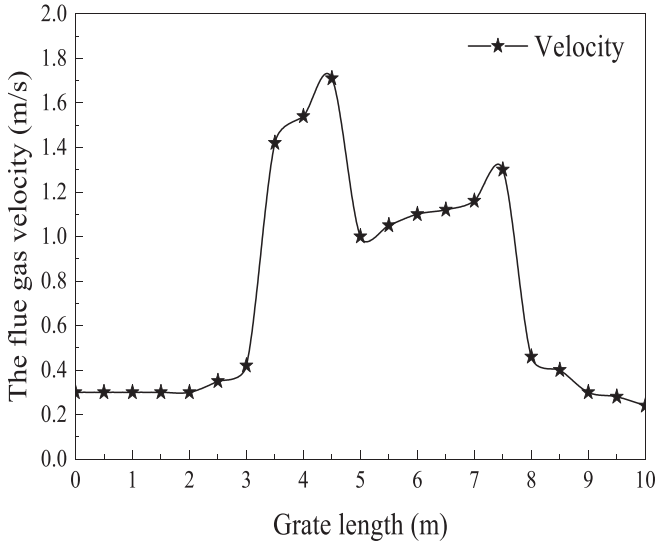

Fig. 4. Flue gas velocity profile along the grate length (the primary inlet is shown in Fig. 1).

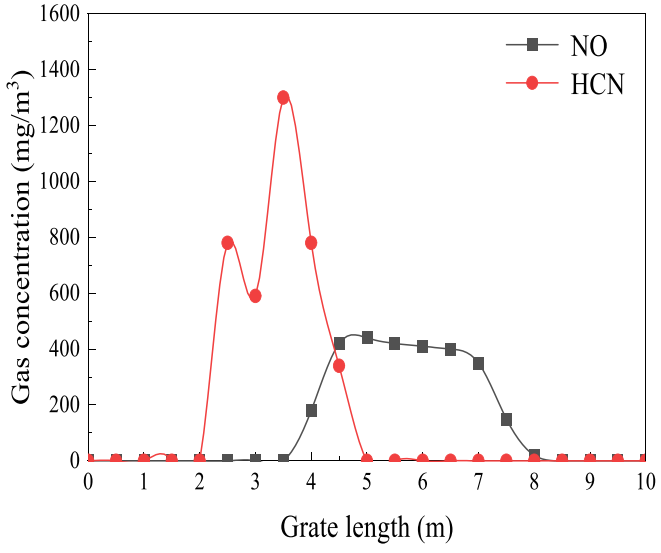

Fig. 6. Concentration distribution of NO and HCN along the bed length (the primary inlet is shown in Fig. 1).

2.5. Model validation

In order to verify the feasibility of the numerical simulation results in this paper, field tests were carried out on the incinerator and relevant data were collected. The average temperature in the middle and outlet of the first flue is measured by the temperature sensor WRKL-5325-4C525/STPT with a range of 0 ~ 1300 ℃ and an error of ± 1.5 ℃. The average temperature at the outlet of the furnace is measured by a sensor of WRKL-5 M25-2 M−1200 with a range of 0 ~ 1300 ℃ and an error of ± 1.5 ℃. The mass fraction of O_2 at the outlet of the furnace is measured by a gas analyzer of Gasboard-9082 with a range of 0 ~ 25 % and an error of less than 3 %. The actual operation data of MSW incinerator is compared with the relevant data of the numerical simulation results, and the results are shown in Table 4.

In this study, we set the actual velocity, temperature, and composition of the bed surface as the boundary conditions for gas-phase combustion in the furnace. This allowed us to determine the combustion rate as it relates to the grate's movement direction.

Table 4
Comparison between the measured data and numerical calculation results of the actual operation of the MSW incinerator.

Parameter	Simulation result	Actual value	Residual (%)
First flue outlet temperature (K)	1218.28	1166.15	4.47
Middle temperature of the first flue (K)	1241.44	1290.75	3.82
Furnace outlet temperature (K)	1282.56	1315.15	2.47
O_2 mass fraction at first flue outlet (%)	6.47	6.70	3.43
NO_x concentration at the first flue outlet (mg/m^3)	155.45	149.71	3.83

Note: the NO_x value has been converted to the defined excess O_2 concentration, which is 6 vol-% (dry flue gas).

Prior to initiating calculations, we estimated the mass fraction of nitrogen in volatiles based on industry waste analysis and elemental analysis. Considering that the generation of instantaneous NO_x

necessitates oxygen rich conditions, and taking into account the combustion conditions of the waste incinerator, we observed that the production of instantaneous NO_x is minimal. Consequently, our simulation primarily focused on thermal NO_x and fuel NO_x. Approximately 90 % of volatile nitrogen was converted into HCN, while the remaining 10 % was converted into NH_3. We conducted a quantitative analysis of nitrogen conversion.

It is worth noting that the reaction scheme involves numerous factors, including chemical equilibrium, reaction rates, activation energy, temperature influence, chemical kinetics, and turbulent mixing all of which impact NO_x generation. Furthermore, we verified the model's accuracy, with the results which are shown in Table 4 revealing errors of 4.47 %, 3.82 %, 2.47 %, 3.43 %, and 3.83 % in comparison to actual values. All errors were below 5 %, underscoring the precision of our simulation results and their ability to effectively mirror the real operation of the incinerator.

2.6. Single-factor simulation test design

In this paper, the secondary air injection angle refers to the angle between the direction of the secondary air injection into the incinerator and the vertical direction of the incinerator (y axis). According to the study [26] on the angle and wind speed of secondary air injection, the influence of the angle of secondary air injection at the rear wall and the wind speed of secondary air injection at the front wall on the NO_x concentration and the thermal efficiency of the incinerator is smaller than that of the angle of secondary air injection at the front wall and the wind speed at the back wall. Therefore, the angle of secondary air injection at the back wall and the wind speed of secondary air injection at the front wall remain unchanged during the single factor test. The magnitude of gas velocity is controlled by the size of the fan air supply, and the gas temperature is controlled by the air–steam preheater. In the present simulation, the secondary air tuyere and the opening area of the secondary air nozzle were kept constant, resulting in different mass flow rates of the secondary air for varying gas velocities. This is because in reality, changing the area of the secondary air tuyere and the opening area of the secondary air nozzle can be challenging.

In establishing simulation conditions for parameters such as the angle of secondary air injection in the front wall, wind speed, and temperature of secondary air injection in the rear wall, we referenced existing experimental and industrial data. These simulation conditions encompass a range of values, and as depicted in the table below, the final values selected for this study fall within these established ranges.

Analysis of the simulation results reveals that when the variation range of the secondary air injection angle is set between 68° and 80°, the NO_x concentration exhibits an initial increase followed by a decrease. Excessive secondary air injection angles lead to more pronounced high-temperature corrosion near the boiler water wall. Therefore, the optimal secondary air injection angle for the front wall is determined to be 80°.

Moreover, as the secondary air injection angle surpasses 80°, NO_x concentration begins to increase again, accompanied by exacerbated high-temperature corrosion near the boiler water wall. Therefore, 80° is identified as the optimal angle.

When considering a range of secondary air speeds from 42 m/s to 66 m/s, the NO_x concentration follows a pattern of initial increase followed by decrease, while the thermal efficiency of the incinerator initially increases, then decreases, and finally increases again. However, it's important to note that as the secondary wind speed increases, the likelihood of the secondary wind flowing to the wall also increases, potentially causing corrosion of the surrounding water wall. Thus, the optimal secondary wind speed is determined to be 66 m/s.

Regarding the secondary air temperature ranging from 293.15 K to 309.15 K, the NOx concentration initially decreases, then increases, and again decreases, while the thermal efficiency of the incinerator first increases and then decreases. Additional simulation was conducted for conditions where the secondary air temperature exceeded 309.15 K, resulting in an observed upward trend in NO_x concentration. However, the improvement in the thermal efficiency of the incinerator was marginal. Consequently, the optimal secondary air temperature is established at 301.15 K. The settings for variable values are shown in Table 5.

Numerical simulation was carried out on the front wall secondary air injection angle (A) of 68°, 70°, 72°, 74°, 76°, 78° and 80°. The rear wall secondary air injection angle was 67°, the secondary wind speed was 42 m/s, and the secondary air temperature was 301.15 K. The NO_x concentration at the outlet (Y_1) and the thermal efficiency (Y_2) of the incinerator were compared under different secondary air injection angles of the front wall. Numerical simulation was carried out for the rear wall secondary air velocity (B) of 42 m/s, 46 m/s, 50 m/s, 54 m/s, 58 m/s, 62 m/s and 66 m/s. The front wall secondary wind speed was 42 m/s, the front wall secondary air injection angle was 74° and 67°, and the temperature of the secondary air was 301.15 K. The NO_x concentration at the outlet and the thermal efficiency of the incinerator were studied under the conditions of different rear wall secondary wind speed. Numerical simulation was carried out on the conditions of secondary air temperature (C) 293.15 K, 297.15 K, 301.15 K, 305.15 K and 309.15 K. The angle of secondary air injection on front and rear walls was 74° and 67° respectively, and the secondary wind speed was 42 m/s. The influence of different secondary air temperature on the NO_x concentration at the outlet and the thermal efficiency of the incinerator was studied. The single factor simulation conditions are shown in Table 6.

In this paper, the thermal efficiency of the incinerator is calculated by the anti-balance method, and the formula of the anti-balance method is as follows:

$$\boldsymbol{\eta} = 100 - (\Delta \boldsymbol{q}_2 + \Delta \boldsymbol{q}_3 + \Delta \boldsymbol{q}_4 + \Delta \boldsymbol{q}_5 + \Delta \boldsymbol{q}_6) \tag{14}$$

The equation used to calculate the heat loss ratio (Δq_2) is as follows:

$$\Delta \boldsymbol{q}_2 = (\boldsymbol{m} + \boldsymbol{n}\boldsymbol{\alpha})\left(\frac{\boldsymbol{T}_{out} - \boldsymbol{T}_{in}}{100}\right)\left(1 - \frac{\boldsymbol{q}_4}{100}\right) \tag{15}$$

The relationship between the volume fraction of CO and the heat loss rate of incomplete combustion of combustible components (Δq_3), as shown in Table 7.

The CO content at the outlet of the first flue was obtained through simulation, and the corresponding heat loss rate of incomplete combustion of combustible components (Δq_3) was selected based on the values given in the Table 7 mentioned above.

The equation used to calculate the heat loss rate of incomplete combustion of solids (Δq_4) is as follows:

$$\Delta \boldsymbol{q}_4 = 337.27\left(\frac{\boldsymbol{ab}}{\boldsymbol{c}(100 - \boldsymbol{b})}\right) \tag{16}$$

The relationship between the rated boiler power and heat dissipation loss Δq_5 when the actual boiler power is not less than 75 % of the rated power, as shown in Table 8.

When the actual operating output of the boiler is less than 75 % of the rated power, the heat dissipation loss ratio Δq_5 can be corrected according to the formula below using the values in the table above:

$$\Delta \boldsymbol{q}_5 = \Delta \boldsymbol{q}_{5ed}\left(\frac{\boldsymbol{D}_{ed}}{\boldsymbol{D}_{sc}}\right) \tag{17}$$

The physical heat loss rate of ash cinder Δq_6 includes heat loss from ash removal and cooling heat loss. Since the ash content studied in this paper is less than the low calorific value of garbage base /418, Δq_6 can be ignored.

Table 5
Settings for Variable Values.

Parameter	Specification
Front wall secondary air injection angle/(°)	60 ~ 80
Secondary wind speed on rear wall/(m/s)	40 ~ 70
Secondary air temperature/(K)	293.15 ~ 313.15

Table 6
Working condition table for single factor simulations.

factor	Parameter	Value
Secondary air injection angle	Front wall secondary air injection angle (°)	68, 70, 72, 74, 76, 78 and 80
	Rear wall secondary air injection angle (°)	67
	Front wall secondary wind speed (m/s)	42
	Rear wall secondary wind speed (m/s)	42
	Secondary air temperature (K)	301.15
Secondary wind speed	Front wall secondary air injection angle (°)	74
	Rear wall secondary air injection angle (°)	67
	Front wall secondary wind speed (m/s)	42
	Rear wall secondary wind speed (m/s)	42, 46, 50, 54, 58, 62 and 66
	Secondary air temperature (K)	301.15
Secondary air temperature	Front wall secondary air injection angle (°)	74
	Rear wall secondary air injection angle (°)	67
	Front wall secondary wind speed (m/s)	42
	Rear wall secondary wind speed (m/s)	42
	Secondary air temperature (K)	293.15, 297.15, 301.15, 305.15 and 309.15

Table 7
The volume fraction of CO is related to the heat loss rate of incomplete combustion Δq_3.

CO volume fraction (%)	Δq_3 (%)
CO ≤ 0.05	0.2
0.05 < CO ≤ 0.1	0.5
CO > 0.1	1.0

Table 8
The relationship between boiler rated power and heat loss Δq_5.

Boiler load rating (t/h)	Δq_5 (%)
≤4	2.9
6	2.4
10	1.7
15	1.5
20	1.3
35	1.1
≥65	0.8

2.7. Optimal design of the response surface test

First, CFD model was used to carry out single factor test, and then the results of single factor test were analyzed, three factors that have significant influence on the NO_x concentration at the outlet and the thermal efficiency of the incinerator are selected to determine the test factors and levels of the response surface. Design Expert 10.0 software was used for the test, and Box-Behnken response surface was selected for optimization analysis [27]. The multivariate quadratic response surface regression model was obtained by analyzing the test results. The single-factor effect analysis was carried out on the multivariate quadratic response surface regression model. The influence curves of each factor on the NO_x concentration at the outlet and the thermal efficiency of the incinerator were obtained by using Expert Design 10.0 software. Then, according to the regression model, the interaction effect of 2 factors on the response surface was analyzed. By fixing 1 factor, the interaction effect between the other two factors was studied. The variation trend between the single factor effect and the double factor effect was compared to obtain the significance of each factor and the double factor influence in the response surface test. Then, the optimal operating parameters were obtained according to the analysis of variance of the test. The method can reflect the interaction of different factors on the experimental results. At the same time, the complex unknown function relationship is fitted by the multivariate quadratic polynomial model in a small area, the calculation is relatively simple, and the prediction model is continuous. Compared with orthogonal test, this method can continuously analyze all levels of the test in the process of optimizing experimental conditions, while orthogonal test can only analyze isolated test points.

3. Single-factor simulation results and analysis

3.1. The influence of the front wall secondary air injection angle on NO_x concentration and thermal efficiency of the incinerator

The O_2 concentration distribution in the central section of the incinerator under various angles of secondary air injection at the front wall (A) is shown in Fig. 7. As the angle of secondary air injection at the front wall is increased, O_2 in the flue occurs closer to the back wall and better agrees with the flow direction of flue gas in the furnace. The influence of the secondary air injection angle at the front wall (A) on the NO_x concentration and thermal efficiency is shown in Fig. 8. The angle of secondary air injection at the front wall significantly influences the NO_x concentration at the outlet and the thermal efficiency of the incinerator. With increasing secondary air injection angle at the front wall, the NO_x concentration at the outlet first increases and then decreases, while the thermal efficiency first increases, then decreases, and finally increases again [28]. This is because, at a low secondary air injection angle on the current wall, the furnace experiences less disturbance, resulting in poor volatile combustion and relatively low NO_x concentration. As the front wall secondary air injection angle increases, combustion around the secondary air inlet becomes more intense, leading to higher NO_x concentration and thermal efficiency in the incinerator. However, when the current wall secondary air injection angle reaches 74°, the rear wall enters a hypoxic state, causing increased turbulence in the furnace and a reduction in NO_x concentration. Beyond an injection angle of 74°, the smoke heat loss initially decreases and then

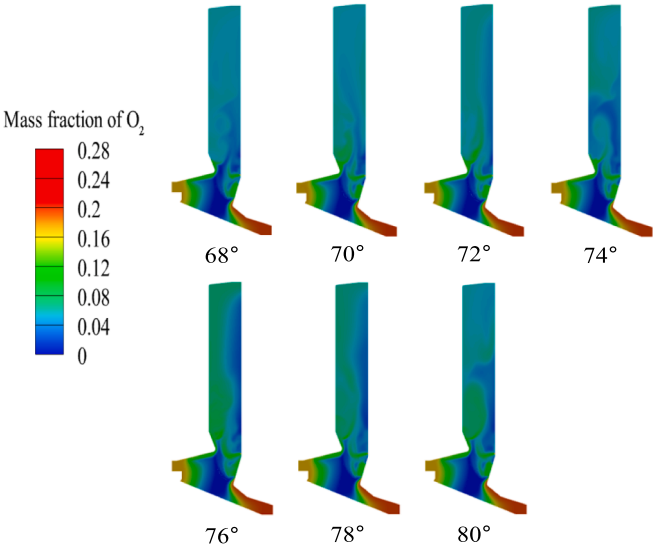

Fig. 7. O_2 concentration distribution in the central section of the incinerator under various angles of secondary air injection of the front wall (A).

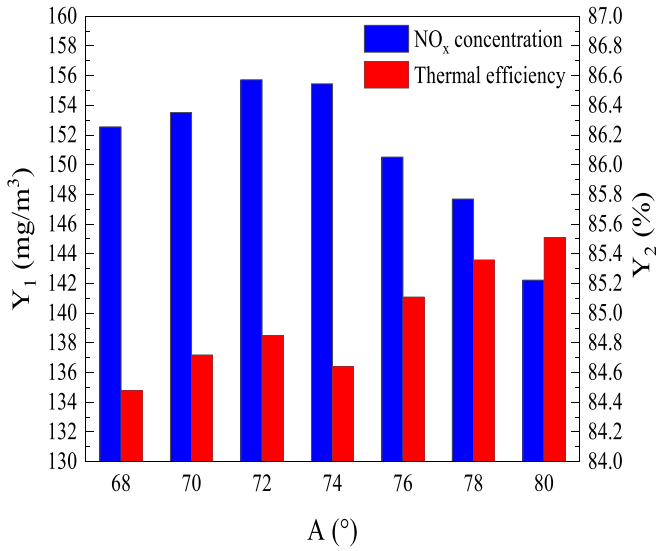

Fig. 8. Influence of the secondary air injection angle of the front wall (A) on the NO_x concentration and thermal efficiency.

increases in the incineration furnace, with the proportion of smoke heat loss becoming the largest. Consequently, the heat efficiency of the incinerator increases once again after the initial reduction. When the secondary air injection angle of the front wall is 80°, the NO_x concentration at the outlet is the lowest, at 142.23 mg/m^3, and the thermal efficiency of the incinerator is also the highest, at 85.51 %. In summary, the optimal secondary air injection angle of the front wall is 80°.

3.2. Influence of the rear wall secondary air velocity on the NO_x concentration and thermal efficiency of the incinerator

The O_2 concentration distribution in the central section of the incinerator under various secondary air velocities of the rear wall (B) is shown in Fig. 9. As shown in Fig. 9, the distribution of O_2 above the grate is not uniform because the amount of oxygen required for waste incineration differs at the four stages of drying, pyrolysis, combustion and burnout. A large amount of oxygen is consumed during combustion, resulting in local anoxia, and secondary air provides a large amount of oxygen, enhancing the combustion of combustible components. The

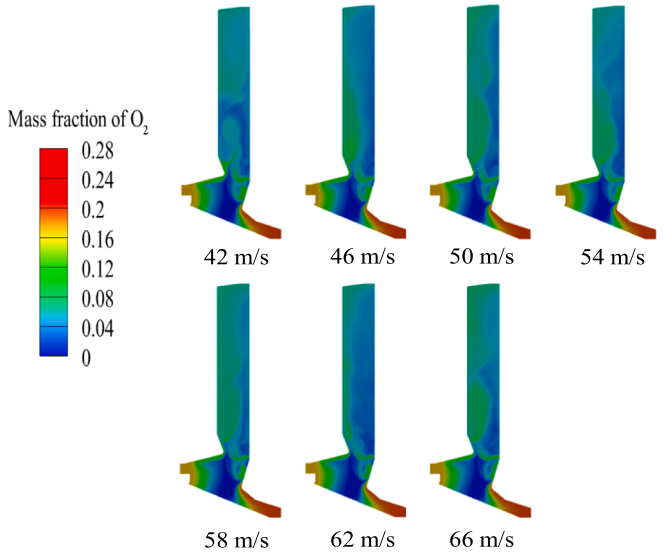

Fig. 9. O_2 concentration distribution in the central section of the incinerator under various velocity of secondary air of rear wall (B).

influence of the secondary air velocity of the rear wall (B) on the NO_x concentration and thermal efficiency is shown in Fig. 10. The rear wall secondary air velocity imposes a significant influence on the NO_x concentration at the outlet and the thermal efficiency of the incinerator. With increasing secondary air velocity of the rear wall, the NO_x concentration at the outlet first increases and then decreases, and the thermal efficiency of the incinerator first decreases, then increases, again decreases and finally increases [29]. This is because when the wind speed of the secondary wind in the back wall increases, it introduces more oxygen and intensifies turbulence within the furnace. This results in more complete combustion of combustible volatile matter in the furnace, leading to an increase in NO_x concentration. However, after the current wind speed of the secondary wind in the wall reaches 46 m/s, the NO_x concentration gradually decreases due to the increased secondary air flow rate. When the secondary air speed on the rear wall increases, the exhaust smoke temperature initially decreases, then increases, and finally decreases again. This fluctuation in smoke temperature leads to a corresponding variation in smoke heat loss within the incineration furnace. Initially, the smoke heat loss decreases, then increases, and eventually decreases once more. The proportion of smoke heat loss in the overall heat loss of the incineration furnace is most significant. As a result, the thermal efficiency of the incinerator follows a pattern of initially increasing, then decreasing, and finally increasing again. When the secondary air velocity of the rear wall is 66 m/s, the NO_x concentration at the outlet is the lowest, at 140.05 mg/m^3, and the thermal efficiency of the incinerator is also the highest, at 85.49 %. Compared to the other working conditions, this may occur because the decrease in the exhaust temperature leads to a reduction in the exhaust heat loss and an increase in the thermal efficiency of the incinerator [30]. After comprehensive analysis, the optimal secondary air velocity of the rear wall is 66 m/s.

3.3. Effect of secondary air temperature on NO_x concentration and thermal efficiency of incinerator

The O_2 concentration distribution in the central section of the incinerator under various secondary air temperatures (C) is shown in Fig. 11. With increasing secondary air temperature, the area with a low O_2 concentration in the flue first moves toward the middle and then toward the wall [31]. The influence of the secondary air temperature (C) on the NO_x concentration and thermal efficiency is shown in Fig. 12. The NO_x concentration at the outlet and the thermal efficiency of the

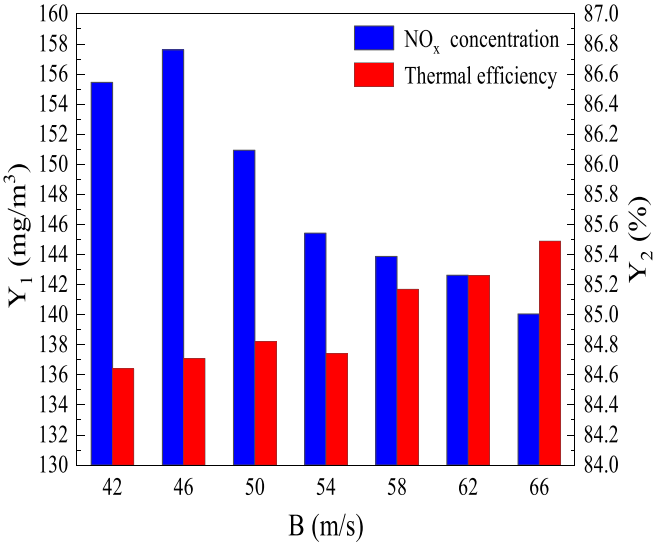

Fig. 10. Influence of secondary air velocity of rear wall (B) on NO_x concentration and thermal efficiency.

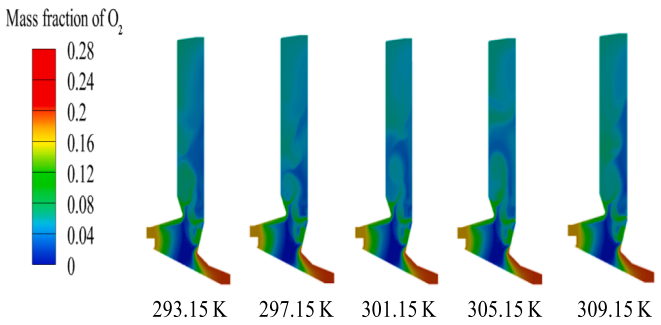

Fig. 11. O_2 concentration distribution in the central section of the incinerator under the various secondary air temperatures (C).

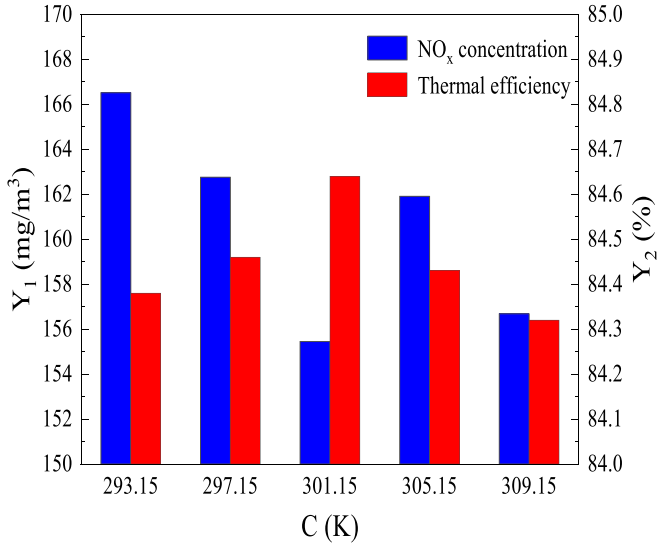

Fig. 12. Influence of the secondary air temperature (C) on the NO_x concentration and thermal efficiency.

incinerator are also obviously affected by the secondary air temperature. When the secondary air temperature is increased, the NO_x concentration at the outlet and the thermal efficiency of the incinerator first decrease, then increase, and finally decrease again [32]. Therefore, the optimal secondary air temperature varies between 297.15 and 305.15 K. This phenomenon occurs because as the temperature of the secondary air rises, the gas density within the furnace decreases, causing an expansion in volume and a subsequent decrease in NO_x concentration. However, when the secondary air temperature reaches 301.15 K, the elevated temperature promotes the generation of thermal NO_x, leading to an increase in NO_x concentration. As the temperature continues to rise, the production of NO_x from fuel-type sources slows down, resulting in a decrease in NO_x concentration once more. When the secondary air temperature is 301.15 K, the NO_x concentration at the outlet is the lowest, at 155.45 mg/m^3. At this time, the thermal efficiency of the incinerator is 84.64 %, which is favorable. After comprehensive analysis, the optimal secondary air temperature is selected as 301.15 K.

4. Response surface test results and analysis

Following the results of single-factor testing, we identified three key factors significantly impacting both the NO_x concentration at the outlet and the thermal efficiency of the incinerator. These factors were chosen as the variables for further testing, and their corresponding levels were determined using Design Expert 10.0 software. We employed the Box-Behnken response surface methodology to optimize our analysis.

By analyzing the experimental results, we derived a multivariate quadratic response surface regression model and performed single-factor effect analysis on this model. Using Design Expert 10.0 software, we generated relationship curves illustrating each factor's influence on both the NO_x concentration at the outlet and the thermal efficiency of the incinerator.

Subsequently, based on the regression model, we conducted a two-factor interaction effect analysis of the response surface. This involved isolating one factor while studying the interaction between the other two. We compared the trends between single-factor effects and double-factor effects to determine the significance of each factor and the combined influence of two factors in the response surface testing.

Finally, we determined the optimal operating parameters through an analysis of variance of the test results.

4.1. Model construction

With the NO_x concentration at the outlet (Y_1) and the thermal efficiency of the incinerator (Y_2) as response values and the front wall secondary air injection angle (A), rear wall secondary air velocity (B) and secondary air temperature (C) as test factors, response surface optimization tests were designed for 17 test points with 3 factors and 3 levels to optimize the secondary air operation parameters of the waste incineration boiler. The Box-Behnken test factors and levels are summarized in Table 9.

The condition Settings in Table 9 are the condition Settings of response surface design, and the condition Settings in Section 3 are the condition Settings of single factor simulation test, which are different. The response surface design process begins with an initial analysis of the individual effects of secondary air injection angle, wind speed, and temperature on both the NO_x concentration at the outlet of the waste incineration boiler and the thermal efficiency of the incinerator. This analysis is conducted through single-factor simulation tests to identify the optimal values for each individual factor. Subsequently, the upper and lower reference values determined during this stage are employed as the basis for establishing three levels within the response surface design. In the next phase, the NO_x concentration at the outlet and the thermal efficiency of the incinerator serve as the response variables. A response surface design comprising 17 test points, with 3 factors at 3 levels each, is employed to optimize the interplay between secondary air injection angle, wind speed, and temperature. This iterative process allows us to derive the optimal operating parameters for the incineration boiler.

Numerical simulation and theoretical calculation were performed to obtain test samples. The test and analysis results are listed in Table 10.

4.2. Significance testing

Design Expert 10.0 software was used to analyze the quadratic regression response of the Box-Behnken test results in Table 4, and the following multivariate quadratic response surface regression model was established:

$$Y_1 = 134.41 + 2.86A - 1.05B + 0.59C + 2.45AB + 1.88AC - 2.01BC + 3.35A^2 + 1.24B^2 + 2.95C^2 \quad (18)$$

Table 9
Box-Behnken test factors and levels.

Element	Level		
	−1	0	1
Front wall secondary air injection angle, A (°)	76	80	84
Rear wall secondary air velocity, B (m/s)	62	66	70
Secondary air temperature, C (K)	297.15	301.15	305.15

Table 10
Box-Behnken test results and analysis.

Test number	A (°)	B (m/s)	C (K)	Y_1 (mg/m^3)	Y_2 (%)
1	76	66	305.15	136.69	86.58
2	76	62	301.15	139.68	85.41
3	80	70	297.15	139.15	84.86
4	84	62	301.15	140.58	85.47
5	80	66	301.15	134.05	85.60
6	84	66	305.15	146.08	85.67
7	84	70	301.15	143.21	84.78
8	80	62	297.15	137.05	86.19
9	76	66	297.15	139.08	86.37
10	80	66	301.15	133.23	85.59
11	80	70	305.15	136.11	86.36
12	80	66	301.15	134.97	85.59
13	76	70	301.15	132.52	86.20
14	80	66	301.15	135.24	85.61
15	80	62	305.15	142.07	84.89
16	80	66	301.15	134.57	85.78
17	84	66	297.15	140.97	85.80

$$Y_2 = 85.63 - 0.36A + 0.03B + 0.035C - 0.37AB - 0.085AC + 0.70BC + 0.18A^2 - 0.35B^2 + 0.29C^2 \quad (19)$$

Variance analysis was conducted of the multivariate quadratic response surface regression model, and the analysis results are provided in Tables 11 and Table 12.

According to the above variance analysis of the multivariate quadratic response surface regression models (Tables 11 and 12), the P values of the multivariate quadratic response surface regression models are all less than 0.01, indicating that the established models are extremely significant. The P values of the missing fitting terms are all greater than 0.05, indicating that the regression models achieve high reliability. The adjustment coefficients of the models R^2_{adj} are 0.9736 and 0.9846, respectively. This indicates that the response value changes exhibit probabilities of 97.36 % and 98.46 %, respectively, and the correlation coefficients R^2 are 0.9885 and 0.9933, respectively, which are similar to the R^2_{adj} values, indicating that the second model yields a suitable fitting degree and small error. According to the above analysis of variance, the three factors influencing the NO_x concentration at the outlet follow the order of A, B and C, i.e., angle of secondary air injection at the front wall > secondary air velocity at the back wall > secondary air temperature. The order of influence of the three factors on the thermal efficiency is A, C and B, i.e., angle of secondary air injection at the front wall > secondary air temperature > secondary air velocity at the back wall.

4.3. Interaction effect analysis of response surface with two factors

In the multivariate quadratic response surface regression model, 1 factor was fixed at the 0 level, and the interaction between the other 2 factors was analyzed in Design Expert 10.0.

The influences of multifactor conditions on the NO_x concentration at the outlet are shown in Fig. 13. As shown in Fig. 13(a), when the secondary air temperature is fixed at the 0 level, under the influence of the secondary air velocity on the rear wall, the change in the NO_x concentration at the outlet shows a trend of first decreasing and then increasing with increasing angle of secondary air injection on the front wall. The curve of the influence of the front wall secondary air injection angle on the NO_x concentration at the outlet changes from gentle to steep, indicating that the secondary air velocity of the back wall greatly influences the front wall secondary air injection angle and the NO_x concentration at the outlet to a certain extent. Under the condition that the secondary wind angle of the front wall is large [33], the NO_x concentration at the outlet first decreases and then increases with the change in the secondary air velocity on the back wall, while the contour line exhibits a closed oval shape, and the response surface exhibits a concave shape. Comprehensive analysis shows that the interaction effect between the secondary air injection angle of the front wall and the secondary air velocity of the back wall exerts an extremely significant influence on the NO_x concentration at the outlet. When the NO_x concentration at the outlet is low, the corresponding reaction conditions vary between 76°~78° and 68 ~ 70 m/s for the secondary air injection angle of the front wall.

As shown in Fig. 13(b), when the secondary air velocity of the rear wall is fixed at the 0 level, the secondary air temperature also greatly influences the secondary air injection angle of the front wall and the NO_x concentration at the outlet [34]. The contour line reflects the variation trend of the water waveform with a secondary air injection angle of the front wall of 78° and a secondary air temperature of 300 K as the center, and the response surface exhibits a concave shape, which indicates that the interaction effect between the secondary air injection angle of the front wall and the secondary air temperature imposes an extremely significant influence on the NO_x concentration at the outlet and reaches a minimum value.

As shown in Fig. 13(c), when the current wall secondary air injection angle is fixed at the 0 level, the influence of the secondary air temperature on the NO_x concentration at the outlet indicates a slow decrease followed by a slow increase [35], with the minimum value varying between 299.15 and 303.15 K. With increasing secondary air temperature, the change trend of the effect of the secondary air temperature on the NO_x concentration at the outlet is consistent with that of the influence of the secondary air velocity of the back wall on the NO_x concentration at the outlet. The contour line also exhibits a closed elliptical trend, and the

Table 11
Quadratic response surface regression model variance analysis for the NO_x concentration at the outlet.

Soruce of variation	Quadratic sum	Degree of freedom	Mean square	F value	P value	Significance
Model	230.20	9	25.58	66.64	< 0.0001	**
A	65.38	1	65.38	170.34	< 0.0001	**
B	8.80	1	8.80	22.93	0.0020	**
C	2.76	1	2.76	7.19	0.0314	*
AB	23.96	1	23.96	62.43	< 0.0001	**
AC	14.06	1	14.06	36.64	0.0005	**
BC	16.24	1	16.24	42.32	0.0003	**
A^2	47.19	1	47.19	122.95	< 0.0001	**
B^2	6.45	1	6.45	16.81	0.0046	**
C^2	36.52	1	36.52	95.16	< 0.0001	**
Residual	2.69	7	0.38			
Loss of quasi item	0.14	3	0.046	0.071	>0.05	
Error term	2.55	4	0.64			
Total	232.89	16				
		$R^2 = 0.9885$		$R^2_{adj} = 0.9736$		

Note: "*" indicates a significant influence on the results (P < 0.05); "**" indicates that the influence on the results is very significant (P < 0.01).

Table 12
Variance analysis of the quadratic response surface regression model for thermal efficiency.

Soruce of variation	Quadratic sum	Degree of freedom	Mean square	F value	P value	Significance
Model	4.52	9	0.50	114.48	< 0.0001	**
A	1.01	1	1.01	229.73	< 0.0001	**
B	0.0072	1	0.0072	1.64	0.2410	
C	0.0098	1	0.0098	2.23	0.1787	
AB	0.55	1	0.55	124.78	< 0.0001	**
AC	0.029	1	0.029	6.59	0.0372	*
BC	1.96	1	1.96	446.61	< 0.0001	**
A^2	0.14	1	0.14	31.26	0.0008	**
B^2	0.51	1	0.51	117.19	< 0.0001	**
C^2	0.36	1	0.36	80.97	< 0.0001	**
Residual	0.031	7	0.0044			
Loss of quasi item	0.0038	3	0.0013	0.19	>0.05	
Error term	0.027	4	0.0067			
Total	4.55	16				
		$R^2 = 0.9933$		$R^2_{adj} = 0.9846$		

Note: "*" indicates a significant influence on the results ($P < 0.05$); "**" indicates that the influence on the results is very significant ($P < 0.01$).

response surface exhibits a concave shape. Comprehensive analysis reveals that the interaction effect between the secondary air velocity on the back wall and the secondary air temperature exerts an extremely significant influence on the NO_x concentration at the outlet.

The influences of multifactor conditions on the thermal efficiency of the incinerator are shown in Fig. 14. As shown in Fig. 14(a), when the secondary air temperature of the front wall is fixed at the 0 level, the secondary air injection angle of the front wall decreases from 84° to 80°, the secondary air velocity on the back wall increases, and the thermal efficiency of the incinerator first increases and then decreases. This occurs because the increase in the secondary air velocity at the beginning provides more O_2, the combustible components in the flue gas are fully burned [36], and the increase in the thermal efficiency of the incinerator gradually increases. As the secondary air velocity at the back wall gradually increased, the air velocity at the outlet also increases, and the heat removed by the flue gas is enhanced, so the thermal efficiency of the incinerator gradually decreases. Therefore, it is necessary to control the secondary air velocity at the back wall within a reasonable range.

As shown in Fig. 14(b), when the secondary air velocity at the back wall is fixed at the 0 level, the secondary air temperature increases in the process of varying the angle of secondary air injection on the front wall, and the thermal efficiency of the incinerator indicates a trend of first decreasing and then increasing [37]. The contour line exhibits a closed oval, which also indicates that the interaction effect between the angle of secondary air injection on the front wall and the secondary air temperature significantly influences the NO_x concentration at the outlet.

According to Fig. 14(c), when the current wall secondary air injection angle is fixed at the 0 level, as the secondary air velocity at the rear wall gradually approaches the minimum value, the secondary air temperature increases, and the thermal efficiency of the incinerator decreases. As the secondary air velocity at the rear wall gradually approaches the maximum value, the secondary air temperature increases, and the thermal efficiency of the incinerator slowly increases. The maximum and minimum secondary air velocities at the rear wall are combined with the secondary air velocity. The thermal efficiency of the incinerator shows the opposite trend. Based on an analysis of the interaction effects, it can be observed that with increasing angle of secondary air injection of the front wall, the decrease in the secondary air velocity of the rear wall, the decrease in the secondary air temperature, and the increase in the thermal efficiency of the incinerator become more significant.

4.4. Response surface model prediction and validation

The relationship between the model-predicted values and actual values is shown in Fig. 15. The closer the actual and predicted values are, the higher the reliability of the model. All the points in Fig. 15(a) and Fig. 15(b) are basically distributed around the 1:1 line, indicating that the two prediction models for the NO_x concentration at the outlet and the thermal efficiency of the incinerator can effectively and highly accurately capture the variation relationship of the 3 factors.

A multivariate quadratic response surface regression model for the NO_x concentration at the outlet and the thermal efficiency of the incinerator, established via the optimization function in Design Expert 10.0 software, was used to analyze the optimal values of the three parameters of the front wall secondary air injection angle, rear wall secondary air velocity and secondary air temperature, as well as the predicted values of the NO_x concentration at the outlet and the thermal efficiency of the incinerator. The analysis results showed that the optimal secondary air parameters obtained by solving the multivariate quadratic response surface regression model for the NO_x concentration at the outlet include a front wall secondary air injection angle of 77.47°, a rear wall secondary air velocity of 69.44 m/s and a rear wall secondary air temperature of 301.84 K. In this case, the predicted NO_x concentration at the outlet is 132.31 mg/m^3. The optimal secondary air parameters obtained with the multivariate quadratic response surface regression model for the incinerator thermal efficiency are as follows: the front wall secondary air injection angle is 84°, the rear wall secondary air velocity is 62 m/s, and the secondary air temperature is 297.15 K. In this case, the predicted incinerator thermal efficiency is 86.49 %.

To verify the response surface model reliability, FLUENT simulations were conducted under the optimal parameter conditions, and the obtained NO_x concentration at the outlet and the incinerator thermal efficiency were compared to the predicted values of the NO_x concentration at the outlet and the incinerator thermal efficiency obtained in Design Expert 10.0 software. To facilitate the actual operation, the optimal secondary air parameters considering the NO_x concentration at the outlet were adjusted as a secondary air injection angle at the front wall of 77°, a secondary air velocity at the back wall of 69 m/s, and a secondary air temperature of 302.15 K. Under these conditions, the NO_x concentration at the outlet reached 134.56 mg/m^3. The error from the model prediction (132.31 mg/m^3) is 1.7 %. Under the condition of the optimal secondary air parameters, the thermal efficiency of the incinerator reached 86.23 %, and the error from the model prediction (86.49 %) is 3.0 %, so the model achieves a high reliability.

4.5. Comprehensive optimization and simulation of the response surface

According to variance analysis, the order of the 3 main influencing factors of the NO_x concentration at the outlet is the angle of secondary air injection at the front wall > secondary air velocity at the back wall > temperature at the rear wall. Therefore, the angle of secondary air injection at the front wall and the secondary air velocity at the back wall

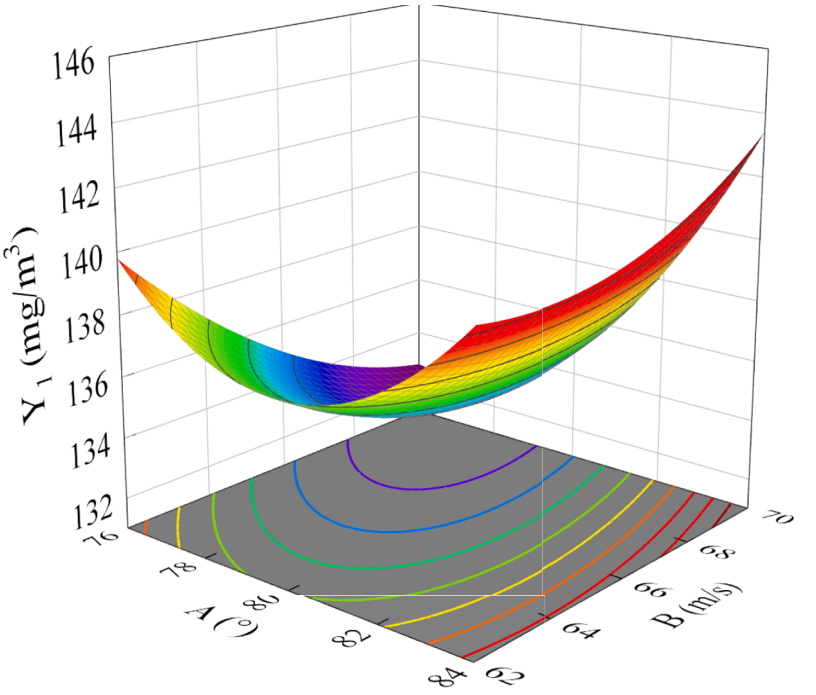

(a)

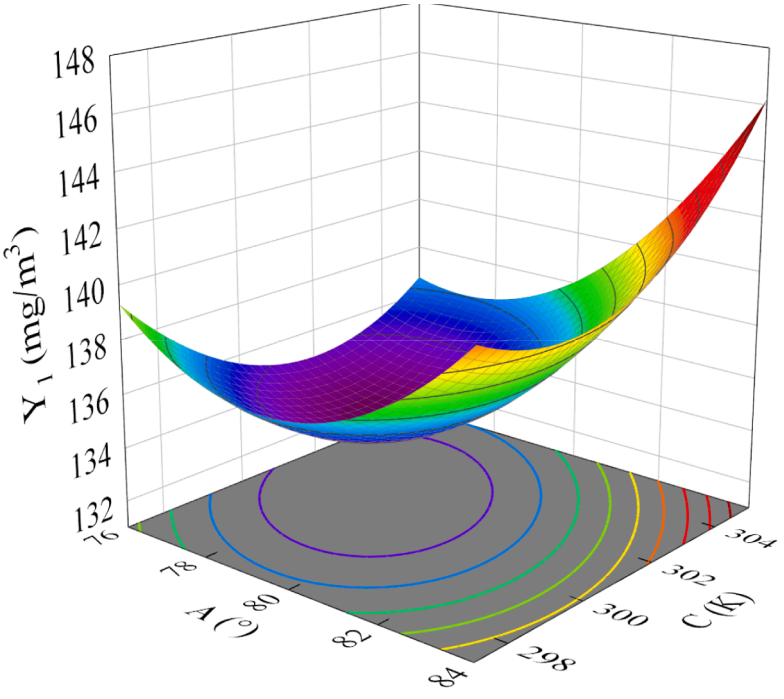

(b)

Fig. 13. Influence of multiple factors on the NO_x concentration at the outlet. (a) Interaction effect between A and B; (b) interaction effect between A and C; (c) interaction effect between B and C.

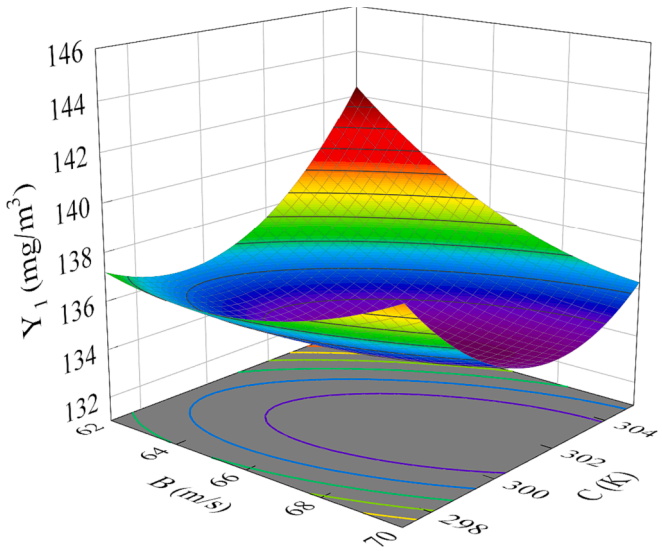

(c)

Fig. 13. (*continued*).

were mainly considered. The order of the 3 main influencing factors of the thermal efficiency of the incinerator is the angle of secondary air injection at the front wall > secondary air temperature > secondary air velocity at the back wall. Therefore, the angle of secondary air injection at the front wall and the secondary air temperature were mainly considered. As shown in Fig. 13(a) and 14(a), the secondary air injection angle of the front wall increases from 77° to 84°, and the NO_x concentration at the outlet first decreases and then increases, but the change is not notable, while the thermal efficiency of the incinerator decreases. Comprehensive analysis revealed that a secondary air injection angle of the front wall of 77° yields a better performance. When the front wall secondary air injection angle is fixed at 77°, the secondary air velocity at the rear wall increases from 62 to 69 m/s, the NO_x concentration at the outlet decreases, and the thermal efficiency of the incinerator increases. Comprehensive analysis showed that a secondary air velocity at the rear wall of 69 m/s yields a better performance. As shown in Fig. 13(b) and 14(b), when the angle of secondary air injection at the front wall is fixed at 77°, the secondary air temperature increases from 297.15 to 302.15 K, and both the NO_x concentration at the outlet and the thermal efficiency of the incinerator decrease, but the NO_x concentration at the outlet decreases less. Comprehensive analysis indicated that a secondary air temperature of 297.15 K is preferable. When the front wall secondary air injection angle is 77°, the rear wall secondary air velocity is 69 m/s, and the secondary air temperature is 297.15 K, numerical simulations were conducted, and the results are presented in Table 13. It can be observed that the NO_x concentration at the outlet is 134.98 mg/m^3, this working condition has a better optimization effect compared to the original working condition, which had a NO_x concentration of 155.45 mg/m^3 at the exit.

This approach offers the advantage of aligning closely with the variations in flue gas temperature, velocity, and composition during actual waste combustion on the grate. Consequently, it yields more precise simulation results with reduced uncertainties. However, it should be noted that converting measured data into simulated boundary conditions can be challenging both in terms of measurement and coding. Nevertheless, the level of accuracy achieved through this method justifies the effort expended.

4.6. Environmental and economic benefits

The incineration scale of the waste incineration power plant in Fuzhou city studied in this paper is 1200 t/d, and the rate of produced flue gas is approximately 7.86 × 10^5 m^3/h. If the operation parameters optimized in this paper were applied to denitrification optimization of the waste incineration power plant, the annual NO_x emission could be reduced by approximately 139.01 t after optimization (7.86 × 10^5 × 20.47 × 24 × 360 × 10^{-9}). There are more than 20 waste incineration power plants using the same type of incinerator in China, with a processing capacity of more than 20,000 t/d, which also indicates that the optimization of secondary air operation parameters in this paper could provide very significant environmental benefits.

The flue gas denitrification technology used in this paper is SNCR denitrification technology [38,39]. Urea is selected as the reducing agent. The urea mixture prepared on site is 40 % high-purity urea, which is sprayed into the incinerator and diluted to approximately 35 % high-purity urea. The denitration efficiency is approximately 45 %, and the ammonia escape rate is approximately 5 %. When urea is used as a reducing agent in the appropriate temperature region, the total reaction equation is:

$$NO + CO(NH_2)_2 + \frac{1}{2}O_2 \rightarrow N_2 + CO_2 + 2H_2O \quad (20)$$

If the operation parameters optimized in this paper were in conjunction with SNCR denitrification, the waste incineration power plant could then save approximately 162.53 t of solid urea particles every year. According to the current market price of solid urea particles of 1800/t, the annual cost could be reduced by approximately ¥ 292,600, with notable economic benefits.

The installed capacity of generators at the waste incineration power plant in Fuzhou studied in this paper is 24 MW. If the operation parameters optimized in this paper were applied to the 2 × 600 t/d incineration boiler of the waste incineration power plant, the annual power generation could be increased by approximately 3.19 × 10^6 kW·h ((calorific value of the burnable waste per kg × improvement value of the incineration equipment conversion efficiency × generator conversion efficiency × annual waste disposal capacity)/kW·h = (1672 × 4186.75 × 0.4 %×95 %×1200 × 1000 × 360)/(3.6 × 10^6)), calculated at a market price of ¥ 0.55/kW·h, which could add approximately ¥

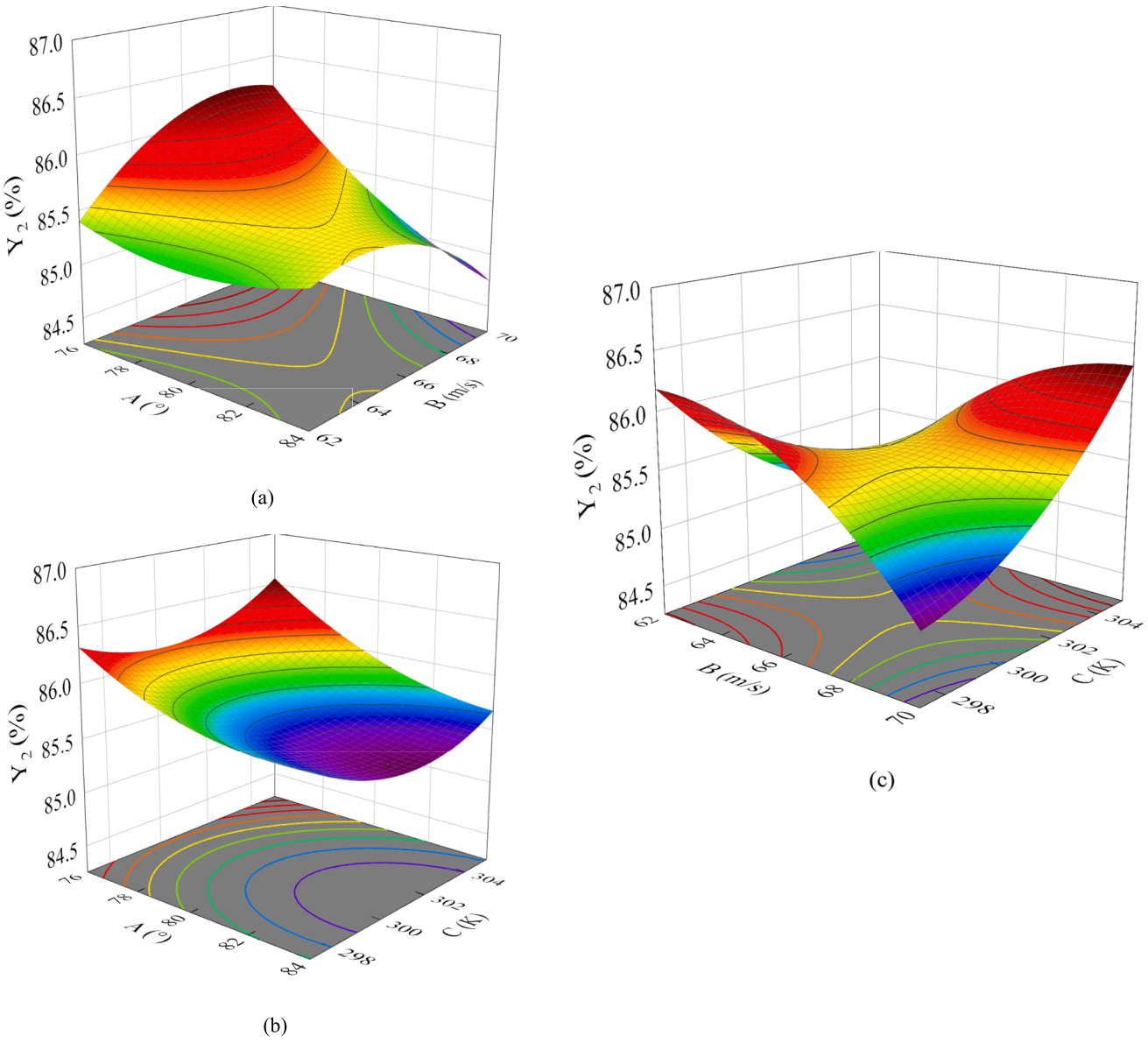

Fig. 14. Influence of multiple factors on thermal efficiency. (a) Interaction effect between A and B; (b) interaction effect between A and C; (c) interaction effect of B and C.

175,000,000 to the economy every year and could provide very significant economic benefits.

While the fuel composition of the waste incineration boiler is indeed complex, and the combustion processes for different fuels vary significantly, it's important to note that the waste materials studied here have undergone extensive investigation and analysis by multiple research groups. This analysis encompasses the waste utilized by the waste incineration power plant throughout the entire year.

Through this comprehensive analysis, it has been determined that the waste processed by the waste incineration power plant originates from various areas within Fuzhou, and the waste source exhibits relative stability. Moreover, the waste sent to the waste incineration plant undergoes a fermentation and breakdown process before reaching the waste incinerator. Consequently, this pre-treatment results in a relatively stable combustion process during boiler operation.

Furthermore, the concentration of urea employed for Selective Non-Catalytic Reduction (SNCR) denitrification is based on actual data obtained from the waste incineration boiler plant. Although this is an estimate derived from a steady-state approximation, it is important to acknowledge that there may be some unaccounted variations. Despite some limitations, our current research suggests that the calculated NO_x emission reduction efficiency is reliable.

5. Conclusions

This work focuses on a single-factor simulation test involving the optimization of secondary air operation parameters of waste incineration boilers, and a multifactor response surface optimization test is then performed, thereby analyzing the influences of the secondary air injection angle, secondary air velocity and secondary air temperature on the NO_x concentration at the outlet and the thermal efficiency of the incinerator. The following conclusions can be obtained:

(1). The simulated outlet temperature of the first flue, the simulated temperature at the middle of the first flue, the simulated outlet temperature of the furnace, the simulated mass fraction of O_2 at the outlet of the first flue and the simulated NO_x concentration at the outlet of the first flue differ by 4.47 %, 3.82 %, 2.47 %, 3.43 %

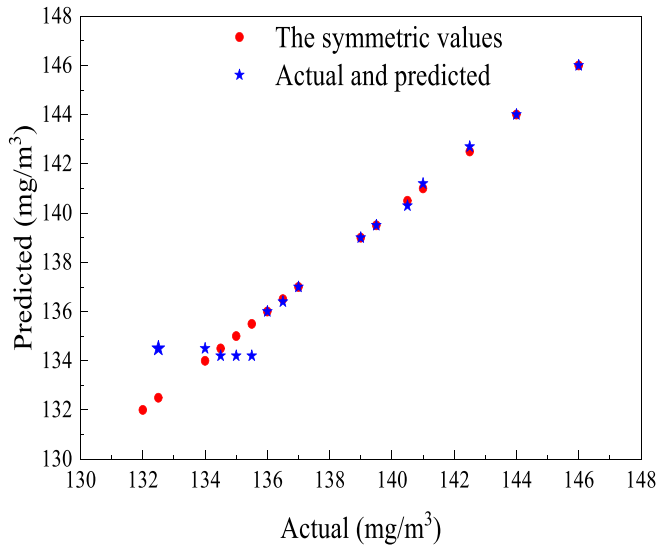

(a)

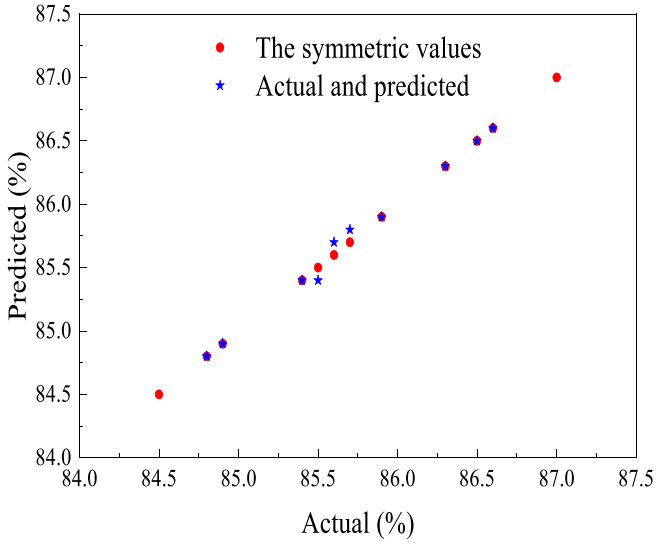

(b)

Fig. 15. Corresponding graph of the predicted and actual value. (a) NO_x concentration at the outlet; (b) thermal efficiency of incinerator.

Table 13
Simulation verifies the optimized operating parameters.

Parameter	Value
NO_x concentration at the exit ($mg \cdot m^{-3}$)	134.98
Thermal efficiency of incinerator (%)	86.11
Furnace flue gas residence time (s)	3.4
Furnace outlet temperature (K)	1233.32
O_2 mass fraction at the exit (%)	6.82

and 3.83 %, respectively, from the actual values, and the errors are all less than 5 %, indicating that the simplified physical model meets the research requirements. The simulation results agree with the actual operating values.

(2). A single-factor simulation test was used to preliminarily optimize the secondary air operation parameters. On the premise of a low NO_x concentration at the outlet and a high thermal efficiency of the incinerator, the preliminary optimized parameters were as follows: the secondary air injection angle of the front wall was 80°, the secondary air velocity at the back wall was 66 m/s, and the secondary air temperature was 301.15 K.

(3). A specific functional relationship between outlet NO_x concentration and thermal efficiency of the incinerator and front wall secondary air injection angle, rear wall secondary air velocity, secondary air temperature has been established. This relationship offers important theoretical support for optimizing the incinerator's secondary air design. For incinerators with different parameters, this function can be further adjusted to match the actual combustion conditions, making the model more representative of real application scenarios.

(4). The simulation test revealed that the NO_x concentration at the outlet is 134.56 mg/m^3, and the thermal efficiency of the incinerator is 86.23 %. Meanwhile, Design Expert 10.0 (State-East company) predicted a NO_x concentration of 132.31 mg/m^3 at the outlet, with a thermal efficiency of 86.49 %. The errors of the simulated and predicted values are 1.7 % and 3.0 %, respectively, indicating high reliability of the model, and that the simulation optimization parameters are more reliable.

(5). Based on the analysis, the optimal operation parameters for the secondary air at the outlet, resulting in better NO_x concentration and thermal efficiency, are a front wall secondary air injection angle of 77°, a rear wall secondary air speed of 69 m/s, and a secondary air temperature of 297.15 K. Under these conditions, the simulation test shows that the NO_x concentration at the outlet is 134.98 mg/m^3, and the thermal efficiency of the incinerator is 86.11 %. This condition has a better optimization effect compared to the original condition, where the NO_x concentration at the exit is 155.45 mg/m3, and the thermal efficiency of the incinerator is 84.64 %.

(6). The research method of optimizing the secondary air parameters of waste incineration boilers via the response surface methodology exhibits a certain feasibility and a practical application value and can be applied to other incineration boilers (different shapes and different designs) to achieve higher environmental and economic benefits.

CRediT authorship contribution statement

Minfeng Zheng: Methodology, Software, Data curation, Investigation, Validation, Writing – original draft, Writing – review & editing. **Jiakang Sun:** Methodology, Software, Data curation, Investigation, Validation, Writing – original draft, Writing – review & editing. **Lingzhu Gong:** Investigation, Funding acquisition. **Yaming Fan:** Investigation, Writing – review & editing. **Jiyuan Tu:** Supervision, Validation, Writing – review & editing. **Jingliang Dong:** Supervision, Validation, Writing – review & editing.

Declaration of Competing Interest

The authors declare that they have no known competing financial interests or personal relationships that could have appeared to influence the work reported in this paper.

Data availability

Data will be made available on request.

Acknowledgement

The authors acknowledge financial support from the Science and Technology Project of Fujian Province (2020Y0055, 2021H6009, 2022I0023), and the Fuzhou Science and Technology Bureau (2021-P-046).

References

[1] S. Chen, J. Huang, T. Xiao, J. Gao, J. Bai, W. Luo, et al., Carbon emissions under different domestic waste treatment modes induced by garbage classification: Case study in pilot communities in Shanghai, China. Sci Total Environ 717 (2020) 137193, https://doi.org/10.1016/j.scitotenv.2020.137193. https://www.ncbi.nlm.nih.gov/pubmed/32062281.

[2] J. Chartier, P.Y. Guernion, I. Milo, CFD modelling of municipal solid waste incineration, Progress in Computational Fluid Dynamics, an International Journal 7 (1) (2007), https://doi.org/10.1504/pcfd.2007.011882.

[3] H.S. Huang, Optimization and Transformation of a 250 t/d MSW Incineration Boiler, Power Equipment 36 (02) (2022) 145–148, https://doi.org/10.19806/j.cnki.fdsb.2022.02.014.

[4] R. Sun, T.M. Ismail, X. Ren, E.-S. Abd, Numerical and experimental studies on effects of moisture content on combustion characteristics of simulated municipal solid wastes in a fixed bed, Waste Manag. 39 (2015) 166–178, https://doi.org/10.1016/j.wasman.2015.02.018. https://www.ncbi.nlm.nih.gov/pubmed/25746177.

[5] Z. Hu, E. Jiang, X. Ma, Numerical simulation on NOX emissions in a municipal solid waste incinerator, J. Clean. Prod. 233 (2019) 650–664, https://doi.org/10.1016/j.jclepro.2019.06.127.

[6] H.H. Frey, B. Peters, H. Hunsinger, J. Vehlow, Characterization of municipal solid waste combustion in a grate furnace, Waste Manag. 23 (8) (2003) 689–701, https://doi.org/10.1016/S0956-053X(02)00070-3. https://www.ncbi.nlm.nih.gov/pubmed/14522187.

[7] J. Wang, W. Fan, Y. Li, M. Xiao, K. Wang, P. Ren, The effect of air staged combustion on NOx emissions in dried lignite combustion, Energy 37 (1) (2012) 725–736, https://doi.org/10.1016/j.energy.2011.10.007.

[8] J. Fu, L. Wei, N. Li, Q. Zhou, T. Liu, Experimental study on temperature, heat flux, strain and stress distribution of boiler water walls, Appl. Therm. Eng. 113 (2017) 419–425, https://doi.org/10.1016/j.applthermaleng.2016.11.039.

[9] M. Yan, W.J. Antoni, D. Hantoko, E. Kanchanatip, Numerical investigation of MSW combustion influenced by air preheating in a full-scale moving grate incinerator, Fuel 285 (2021), https://doi.org/10.1016/j.fuel.2020.119193.

[10] B. Rajh, C. Yin, N. Samec, M. Hribersek, F. Kokalj, M. Zadravec, Advanced CFD modelling of air and recycled flue gas staging in a waste wood-fired grate boiler for higher combustion efficiency and greater environmental benefits, J. Environ. Manage. 218 (2018) 200–208, https://doi.org/10.1016/j.jenvman.2018.04.030. https://www.ncbi.nlm.nih.gov/pubmed/29680752.

[11] Y.B. Yang, H. Yamauchi, V. Nasserzadeh, J. Swithenbank, Effects of fuel devolatilisation on the combustion of wood chips and incineration of simulated municipal solid wastes in a packed bed☆, Fuel 82 (18) (2003) 2205–2221, https://doi.org/10.1016/s0016-2361(03)00145-5.

[12] J. Li, W. Yang, W. Blasiak, A. Ponzio, Volumetric combustion of biomass for CO2 and NOx reduction in coal-fired boilers, Fuel 102 (2012) 624–633, https://doi.org/10.1016/j.fuel.2012.06.083.

[13] G.H. Liu, X.Q. Ma, Z. Yu, Experimental and kinetic modeling of oxygen-enriched air combustion of municipal solid waste, Waste Manag. 29 (2) (2009) 792–796, https://doi.org/10.1016/j.wasman.2008.06.010. https://www.ncbi.nlm.nih.gov/pubmed/18691862.

[14] A. Zhou, H. Xu, Y. Tu, F. Zhao, Z. Zheng, W. Yang, Numerical investigation of the effect of air supply and oxygen enrichment on the biomass combustion in the grate boiler, Appl. Therm. Eng. 156 (2019) 550–561, https://doi.org/10.1016/j.applthermaleng.2019.04.053.

[15] X.X. Ning, X.Q. Ma, Z.F. Hu, S.S. Yu, Y.F. Liao, Numerical simulation of deep staged-air distribution of municipal solid waste incinerator, Environ. Pollut. Cont. 38 (10) (2016) 53–60, https://doi.org/10.15985/j.cnki.1001-3865.2016.10.010.

[16] H.C. Wang, X.H. Zeng, Y.F. Liao, Y.L. Tian, Numerical simulation on air distribution optimization of large municipal solid waste incinerator, Chemical Engineering & Equipment 02 (2020) 10–11, https://doi.org/10.19566/j.cnki.cn35-1285/tq.2020.02.004.

[17] X.L. Huai, W.L. Xu, Z.Y. Qu, Z.G. Li, F.P. Zhang, G.M. Xiang, et al., Numerical simulation of municipal solid waste combustion in a novel two-stage reciprocating incinerator, Waste Manag. 28 (1) (2008) 15–29, https://doi.org/10.1016/j.wasman.2006.11.010. https://www.ncbi.nlm.nih.gov/pubmed/17236753.

[18] J.W. Lu, S. Zhang, J. Hai, M. Lei, Status and perspectives of municipal solid waste incineration in China: A comparison with developed regions, Waste Manag. 69 (2017) 170–186, https://doi.org/10.1016/j.wasman.2017.04.014. https://www.ncbi.nlm.nih.gov/pubmed/28408280.

[19] M. Markovic, E.A. Bramer, G. Brem, Experimental investigation of wood combustion in a fixed bed with hot air, Waste Manag. 34 (1) (2014) 49–62, https://doi.org/10.1016/j.wasman.2013.09.021. https://www.ncbi.nlm.nih.gov/pubmed/24125795.

[20] F.O. Centeno-González, E.E. Silva Lora, H.F. Villa Nova, L.J. Mendes Neto, A. M. Martínez Reyes, A. Ratner, et al., CFD modeling of combustion of sugarcane bagasse in an industrial boiler, Fuel 193 (2017) 31–38, https://doi.org/10.1016/j.fuel.2016.11.105.

[21] S. Chapela, J. Porteiro, M. Costa, Effect of the turbulence-chemistry interaction in packed-bed biomass combustion, Energy Fuel 31 (9) (2017) 9967–9982, https://doi.org/10.1021/acs.energyfuels.7b00516.

[22] M. Costa, N. Massarotti, V. Indrizzi, B. Rajh, C. Yin, N. Samec, Engineering bed models for solid fuel conversion process in grate-fired boilers, Energy 77 (2014) 244–253, https://doi.org/10.1016/j.energy.2014.07.067.

[23] T. Nussbaumer, M. Kiener, P. Horat, Fluid dynamic optimization of grate boilers with scaled model flow experiments, CFD modeling, and measurements in practice, Biomass Bioenergy 76 (2015) 11–23, https://doi.org/10.1016/j.biombioe.2015.02.033.

[24] H. Shi, D. Wang, Numerical simulation of nitrogen oxide emission characteristics of a retrofitted chain grate boiler, Chem. Technol. Fuels Oils 53 (4) (2017) 610–620, https://doi.org/10.1007/s10553-017-0841-3.

[25] Z. Hu, E. Jiang, X. Ma, Numerical simulation on operating parameters of SNCR process in a municipal solid waste incinerator, Fuel 245 (2019) 160–173, https://doi.org/10.1016/j.fuel.2019.02.071.

[26] ZJ. Zou, JK. Sun, MF. Zheng, LZ. Gong, Study on the influence of secondary air on combustion process and NOx pollution control of waste incineration boiler, Chemical Engineering & Equipment 4 (2023) 235238, https://doi.org/10.19566/j.cnki.cn35-1285/tq.2023.04.050.

[27] A. Wu, Y. Wu, G.J. Li, X.B. Li, Z.M. Zhang, Process design and multi-geometric parameter optimization of large conical parts based on response surface method, Journal of Mechanical Engineering 55 (24) (2019) 83–92. https://kns.cnki.net/kcms/detail/11.2187.TH.20191202.2011.092.html.

[28] Z. Hu, X. Ma, Y. Chen, Y. Liao, J. Wu, Z. Yu, et al., Co-combustion of coal with printing and dyeing sludge: Numerical simulation of the process and related NO_x emissions, Fuel 139 (2015) 606–613, https://doi.org/10.1016/j.fuel.2014.09.047.

[29] I.A. Shah, X. Gou, Q. Zhang, J. Wu, E. Wang, Y. Liu, Experimental study on NOx emission characteristics of oxy-biomass combustion, J. Clean. Prod. 199 (2018) 400–410, https://doi.org/10.1016/j.jclepro.2018.07.022.

[30] H. Lin, X. Ma, Simulation of co-incineration of sewage sludge with municipal solid waste in a grate furnace incinerator, Waste Manag. 32 (3) (2012) 561–567, https://doi.org/10.1016/j.wasman.2011.10.032. https://www.ncbi.nlm.nih.gov/pubmed/22119515.

[31] C. Jordan, M. Harasek, Improvement of a combustion unit based on a grate furnace for granular dry solid biofuels using CFD methods, Heat Transfer Eng. 31 (9) (2010) 774–781, https://doi.org/10.1080/01457630903501062.

[32] W. Yang, B. Wang, S. Lei, K. Wang, T. Chen, Z. Song, et al., Combustion optimization and NO_x reduction of a 600 MWe down-fired boiler by rearrangement of swirl burner and introduction of separated over-fire air, J. Clean. Prod. 210 (2019) 1120–1130, https://doi.org/10.1016/j.jclepro.2018.11.077.

[33] M. Costa, M. Dell'isola, N. Massarotti, Numerical analysis of the thermo-fluid-dynamic field in the combustion chamber of an incinerator plant, Energy 34 (12) (2009) 2075–2086, https://doi.org/10.1016/j.energy.2008.08.024.

[34] Y.B. Yang, C.N. Lim, J. Goodfellow, V.N. Sharifi, J. Swithenbank, A diffusion model for particle mixing in a packed bed of burning solids, Fuel 84 (2–3) (2005) 213–225, https://doi.org/10.1016/j.fuel.2004.09.002.

[35] Y.B. Yang, R. Newman, V. Sharifi, J. Swithenbank, J. Ariss, Mathematical modelling of straw combustion in a 38MWe power plant furnace and effect of operating conditions, Fuel 86 (1–2) (2007) 129–142, https://doi.org/10.1016/j.fuel.2006.06.023.

[36] J. Wang, Y. Xue, X. Zhang, X. Shu, Numerical study of radiation effect on the municipal solid waste combustion characteristics inside an incinerator, Waste Manag. 44 (2015) 116–124, https://doi.org/10.1016/j.wasman.2015.07.025. https://www.ncbi.nlm.nih.gov/pubmed/26233882.

[37] C. Ryu, D. Shin, S. Choi, Combined simulation of combustion and gas flow in a grate-type incinerator, J. Air Waste Manag. Assoc. 52 (2) (2002) 189–197, https://doi.org/10.1080/10473289.2002.10470769. https://www.ncbi.nlm.nih.gov/pubmed/15143794.

[38] T.D.B. Nguyen, T.-H. Kang, Y.-I. Lim, W.-H. Eom, S.-J. Kim, K.-S. Yoo, Application of urea-based SNCR to a municipal incinerator: On-site test and CFD simulation, Chem. Eng. J. 152 (1) (2009) 36–43, https://doi.org/10.1016/j.cej.2009.03.025.

[39] Z. Xia, J. Li, T. Wu, C. Chen, X. Zhang, CFD simulation of MSW combustion and SNCR in a commercial incinerator, Waste Manag. 34 (9) (2014) 1609–1618, https://doi.org/10.1016/j.wasman.2014.04.015. https://www.ncbi.nlm.nih.gov/pubmed/24863625.